

Dissociation and thermodynamical properties of heavy quarkonia in an anisotropic strongly coupled hot quark gluon plasma: Using a baryonic chemical potential

Siddhartha Solanki , Manohar Lal, Rishabh Sharma , and Vineet Kumar Agotiya *

Department of Physics, Central University of Jharkhand, Ranchi 835222, India

 (Received 27 July 2023; revised 18 September 2023; accepted 23 October 2023; published 6 February 2024)

Background: In the production of hot quark gluon plasma in high-energy heavy-ion collisions, the charmonium binding in the deconfined interior is prevented by color screening. The formation of deconfining plasma was found as a signature of reduction of the charmonium (a bound state of charm and anticharm quark) production. A significant amount of charm suppression has been observed in heavy-ion collisions (p -A) in various experimental investigations. Some of the issues are still not clear in this area of research, such as the study of hadronic properties in dense nuclear matter, the deconfinement phase transition from hadronic to quark gluon matter, etc. We follow up on the recently published work of Jamal *et al.* [M. Y. Jamal, I. Nilima, V. Chandra, and V. K. Agotiya, *Phys. Rev. D* **97**, 094033 (2018)]; in this work the authors calculated the properties of quarkonia [i.e., potential, binding energy, and dissociation temperature (using thermal width criteria)] in the presence of temperature and anisotropy.

Purpose: To investigate the properties of quarkonia, namely, potential, binding energy, mass spectra, dissociation temperature (using thermal width and thermal energy criteria), and thermodynamical properties of quark gluon plasma (i.e., pressure, energy density, and speed of sound) in the presence of baryonic chemical potential (μ_b) and anisotropy (ξ).

Methods: The properties of quarkonia and the thermodynamical properties of quark gluon plasma (QGP) are calculated by using the quasiparticle approach with μ_b in hot quantum chromodynamics medium. The medium modified form of heavy-quark potential at finite values of μ_b and ξ is considered. The calculations have been done by considering the real and imaginary parts of the potential with a static gluon propagator. The real part of the potential has been used in solving the Schrödinger equation to obtain the binding energy of quarkonia, and the imaginary part gives rise to the thermal width of heavy quarkonia.

Results: The binding energy and the dissociation temperature of S states of charmonia and bottomonia for $n = 1$ and $n = 2$ (radial quantum number) and the mass spectra of $1S$ states of quarkonia with the effects of μ_b and ξ were calculated. The thermodynamical properties of QGP using the parameters ξ and μ_b were also determined. It was noticed that, with an increase in the value of μ_b , the values of the associated properties of quarkonia decrease. On the other hand, by increasing the value of ξ , the values of the properties of quarkonia increase. The extracted values of mass spectra and the variation of thermodynamical properties of QGP are also compared with the recently published theoretical and experimental data and a reasonable agreement between these values is observed.

Conclusions: We have studied the properties of quarkonium state (i.e., $1S$ and $2S$ -states) and the thermodynamical properties of QGP with μ_b and ξ in hot and dense quantum chromodynamics medium. Finally with this, we may conclude that the obtained result (mention in result section) might be helpful for enhancing studies of the highly dense object (because Compressed Baryonic Matter experiment at the Facility for Anti-proton and ion Research in exploring QGP at higher baryon densities).

DOI: [10.1103/PhysRevC.109.024905](https://doi.org/10.1103/PhysRevC.109.024905)

I. INTRODUCTION

Experiments using various particle accelerators, viz., the Relativistic Heavy-Ion Collider (RHIC) at Brookhaven Na-

*agotiya81@gmail.com

Published by the American Physical Society under the terms of the [Creative Commons Attribution 4.0 International](https://creativecommons.org/licenses/by/4.0/) license. Further distribution of this work must maintain attribution to the author(s) and the published article's title, journal citation, and DOI. Funded by SCOAP³.

tional Laboratory (BNL), USA, and the CERN Large Hadron Collider (LHC), Switzerland, have inferred that quark gluon plasma (QGP) behaves like a perfect fluid instead of a non-interacting gas of quasipartons and quasiglons due to its collective nature [1–3]. Several signatures of QGP have been identified so far but suppression of the quark-antiquark pair is one of the most important or confirming signals of QGP formation during noncentral collision of heavy ions [4,5]. Matsui and Satz [6] were the first to study the dissociation of quarkonia, particularly that of charmonia (J/ψ), by employing color screening in a deconfined state. Both experimental and theoretical studies exploring the properties of QGP are

under way, and a few essential refinements in the study of QGP have been observed during the past few decades [6–8]. It is well known that a quarkonium is bound together by static gluons and acts as an independent degree of freedom [9–12]. Light hadrons were emitted during the transition of a quarkonium from one state to another state while passing through the QGP medium [13]. Various authors [13–15] have studied the features of quantum chromodynamics (QCD), a strong theory of interaction, at a high-temperature scale. Studies like Refs. [16–18] are dedicated to quarkonium production in a color evaporation model or a color-singlet model. The suppression of QGP through coalescence or the recombination of partons can be found in Refs. [19,20]. Due to the small velocity or large mass of heavy quarks compared to QCD scale parameters, a nonrelativistic approach was preferably used to study QGP properties [21–23]. In this approach, a nonrelativistic potential is employed that possesses two fundamental features, i.e., asymptotic freedom and color confinement of the QCD. Studies (both theoretical and experimental) exist in the literature [24–30] that are focused on the properties (including dissociation temperature), production, and suppression of QGP. The dissociation temperature of states has been investigated by using a quasiparticle approach in the presence of the momentum anisotropy collision [31]. Several other studies [28–30,32–34] have included the anisotropic effect to explore QGP.

The key idea in the present work is to include the effect of the baryonic chemical potential along with the anisotropic one in the hot QGP medium using an effective fugacity quasiparticle model. The effect of the momentum space has been incorporated through the distribution function, the details of which can be found in Refs. [9,35,36]. The gluon propagator and the dielectric permittivity were modified in the presence of anisotropy (ξ). The effect of the chemical potential has been introduced through quasiparticle Debye mass [37,38]. In the present work, the potential has been modified accordingly. From the real part of the potential, so formed, the binding energies of charmonia and bottomonia were obtained at different values of anisotropy [11,39–43]. The thermal width of QGP has been derived from the imaginary part of the potential [11,39–43]. In previous studies, such as Refs. [44–47], the authors have calculated the dissociation temperature by using the criterion of thermal width. This idea inspired us to study the binding energy and the thermal width of QGP particularly at high baryon density (baryonic chemical potential). The effects of the baryonic chemical potential and anisotropy significantly revise the values of the dissociation temperature. The thermodynamical behavior of QGP in the presence of μ_b and ξ has also been studied. Various thermodynamical quantities of QGP such as pressure, energy density, and speed of sound have been studied. These quantities played a vital role in studying the suppression of QGP, which is regarded as the most prominent signal for the existence of QGP.

The present paper is organized as follows. A brief discussion about the theoretical framework used in the present work is provided in Sec. II. In Sec. III, the calculations and results obtained are presented, and finally, the summary and conclusions of the present work are given in Sec. IV.

II. THEORETICAL FRAMEWORKS USED IN THE PRESENT WORK

A. Study of quasiparticle Debye mass with baryonic chemical potential and temperature

Unlike quantum electrodynamics, the Debye mass (m_D) in the case of QCD is nonperturbative and gauge invariant. The leading-order Debye mass in QCD coupling at high temperatures has been known for a long time and is perturbative in nature. Rebhan *et al.* [48] have defined the Debye mass by seeing the pole of the static propagator that is relevant, instead of the time-time component of the gluon self-energy, and have obtained a Debye mass that is gauge independent. This is due to the fact that the pole of self-energy does not depend on the choice of the gauge. The Debye mass was calculated for QGP at a high temperature next to leading order in QCD coupling from the correlation of two Polyakov loops by Braaten and Nieta [49]; this result agrees with the Hard Thermal Loop (HTL) result [48]. It was pointed out by Arnold and Zhai [50] that the physics of the confined magnetic charge has to be known in order to understand the contribution of $O(g^2 T)$ to the Debye mass in QCD; it was also pointed out by them that the Debye mass as a pole of the gluon propagator no longer holds true. Importantly in lattice QCD, the definition of the Debye mass itself encounters difficulty due to the fact that unlike QED the electric field correlators are not gauge invariant in QCD. The proposal of this problem is based on effective theories obtained by dimensional reduction [51], the spatial correlation function of gauge-invariant meson energy, and the behavior of color-singlet free energies [52]. Burnier and Rothkopf [53] have attempted to define a gauge-invariant mass from a complex static in-medium heavy-quark potential obtained from lattice QCD. Several attempts have been made to capture all the interaction effects present in the hot QCD equation of state (EoS) in terms of noninteracting quasipartons (quasigluons and quaquarks). These quasipartons are the excitations of the interacting quarks and gluons and there are several models that describe the quasipartons, such as the effective mass model [54,55], the effective mass model with a Polyakov loop [56], models based on Polyakov-loop-extended Nambu-Jona-Lasinio model (PNJL) and Nambu-Jona-Lasinio model (NJL) [57], and the effective fugacity model [58,59]. In QCD the quasiparticle model is a phenomenological model that is widely used to describe the nonlinear behavior of QGP near the phase transition point. In this model, a system of interacting massless quarks and gluons can be described as an ideal gas of massive noninteracting quasiparticles. The mass of the quasiparticle is dependent on the temperature, which rises due to the interaction of gluons and quarks with the surrounding medium. The quasiparticle retains the quantum number of the quarks and gluons [60]. In our calculation, we used the Debye mass (m_D) for the full QCD case [32], which is given by

$$\frac{m_D^2(T)}{g^2(T)T^2} = \left[\left(\frac{N_c}{3} \times \frac{6\text{PolyLog}[2, z_g]}{\pi^2} \right) + \left(\frac{\hat{N}_f}{6} \times \frac{-12\text{PolyLog}[2, -z_q]}{\pi^2} \right) \right] \quad (1)$$

and

$$\hat{N}_f = \left(N_f + \frac{3}{\pi^2} \sum \frac{\mu_b^2}{9T^2} \right). \quad (2)$$

Here, $g(T)$ is the temperature-dependent two-loop running coupling constant, $N_c = 3$ [SU(3)], N_f is the number of flavors, the function $\text{PolyLog}[2, z]$ has the form $\text{PolyLog}[2, z] = \sum_{k=1}^{\infty} \frac{z^k}{k^2}$, z_g is the quasigluon effective fugacity, and z_q is the quaquark effective fugacity. These distribution functions are isotropic in nature,

$$f_{g,q} = \frac{z_{g,q} \exp(-\beta p)}{[1 \pm z_{g,q} \exp(-\beta p)]}, \quad (3)$$

where g stands for quasigluons and q for quaquarks. These fugacities should not be confused with any conservation laws (number conservation) and have merely been introduced to encode all the interaction effects at high-temperature QCD. Both z_g and z_q have a very complicated temperature dependence and asymptotically reach the ideal value unity [59]. The temperature-dependent z_g and z_q fits well into the following form,

$$z_{g,q} = a_{q,g} \exp\left(-\frac{b_{g,q}}{x^2} - \frac{c_{g,q}}{x^4} - \frac{d_{g,q}}{x^6}\right) \quad (4)$$

(here, $x = T/T_c$ and $a, b, c,$ and d are fitting parameters) for both EoS1 and EoS2. EoS1 is the $O(g^5)$ hot QCD EoS [50] and EoS2 is the $O[g^6 \ln(1/g)]$ hot QCD EoS [51] in the quasiparticle description [58,59], respectively. Now, the final expressions of the full QCD case or the quasiparticle Debye mass in terms of the baryonic chemical potential and the temperature [37,38] can be written as

$$\frac{m_D^2(T, \mu_b)}{T^2} = \left(\left\{ \frac{N_c}{3} Q_g^2 \right\} + \left\{ \left[\frac{N_f}{6} + \frac{1}{2\pi^2} \left(\frac{\mu_b^2}{9T^2} \right) \right] Q_q^2 \right\} \right), \quad (5)$$

where μ_b is the baryonic chemical potential, and Q_g and Q_q are the effective charges given by the following equations:

$$Q_g^2 = g^2(T) \frac{6 \text{PolyLog}[2, z_g]}{\pi^2},$$

$$Q_q^2 = g^2(T) \frac{-12 \text{PolyLog}[2, -z_q]}{\pi^2}. \quad (6)$$

In our analysis, the temperature- and baryonic-chemical-potential-dependent quasiparticle Debye mass [i.e., $m_D(T, \mu_b) \equiv m_D$ or $m_D^2(T, \mu_b) \equiv m_D^2$] has been employed to deduce the binding energy, the mass spectra, the dissociation temperature of the quarkonia states, and the thermodynamical properties of QGP.

B. Modification of the Cornell potential using Fourier transform (FT)

The velocity of the heavy-quark mass in the bound state is small because of the large quark mass ($m = m_{c,b} \geq \Lambda_{\text{QCD}}$), and the binding effects in quarkonia at the value of zero temperature can be understood in terms of nonrelativistic potential models [61]. At zero temperature, the vacuum potential (the Cornell potential) is given as

$$V(r) = -\frac{\alpha}{r} + \sigma r, \quad (7)$$

where σ and α denote the string tension and the two-loop coupling constant, respectively. Because the one-dimensional vacuum potential defined by Eq. (7) is valid at zero temperature, to study the QGP at finite temperature, modification of the Cornell potential is required and this is done by using Fourier transform (FT). The medium modification enters into this heavy-quark potential $V(k)$ via FT [62] as below:

$$\tilde{V}(k) = \frac{\tilde{V}(k)}{\epsilon(k)}, \quad (8)$$

where k is the Fourier conjugate of the interquark distance (r) and the dielectric permittivity $[\epsilon(k)]$ is obtained by the static limit of the longitudinal part of the gluon self-energy [63,64] as

$$\epsilon(k) \equiv \left(1 + \frac{m_D^2(T, \mu_b)}{k^2} \right), \quad (9)$$

where $m_D^2(T, \mu_b)$ is the notation of the quasiparticle or the full QCD Debye mass with the dependency of the baryonic chemical potential and the temperature defined by Eq. (5). $V(k)$ is the FT of the Cornell potential in Eq. (8). Obtaining the FT of Eq. (7), the Cornell potential, is not an easy job. Therefore, we consider r as distribution. Then the FT of the Coulombic part is straightforward to compute. The FT of the linear part $\sigma r \exp(-\gamma r)$ is

$$\text{FT}[\sigma r \exp(-\gamma r)] = -\frac{i\sigma}{k\sqrt{2\pi}} \left(\frac{2}{(\gamma - ik)^3} - \frac{2}{(\gamma + ik)^3} \right). \quad (10)$$

At $\gamma = 0$, we find the FT of σr is

$$\text{FT}(\sigma r) = -\frac{4\sigma}{k^4\sqrt{2\pi}}. \quad (11)$$

The medium correction to the potential after applying the inverse FT reads as

$$V(r) = \int \frac{d^3\mathbf{k}}{(2\pi)^{3/2}} (e^{i\mathbf{k}\cdot\mathbf{r}} - 1) \tilde{V}(k). \quad (12)$$

The FT of the Cornell potential is

$$\tilde{V}(k) = -\sqrt{\frac{2}{\pi}} \left(\frac{\alpha}{k^2} + 2\frac{\sigma}{k^4} \right). \quad (13)$$

Now substituting Eqs. (9) and (13) in Eq. (8), and employing the inverse FT, we get the medium modified form of the potential [58,62,63,65] depending upon distance (r) as below:

$$V(r, T, \mu_b) = \left(\frac{2\sigma}{m_D^2(T, \mu_b)} - \alpha \right) \frac{\exp[-m_D(T, \mu_b)r]}{r}$$

$$- \frac{2\sigma}{m_D^2(T, \mu_b)r} + \frac{2\sigma}{m_D(T, \mu_b)} - \alpha m_D(T, \mu_b). \quad (14)$$

It is also noticeable that in a hot QCD medium, the expression of the potential is not the same as the lattice parametrized heavy-quark free energy in the deconfined phase (which is basically a screened Coulomb, more details can be found in Ref. [66]). As emphasized by Dixit [67], a one-dimensional FT of the Cornell potential in the medium yields a form

similar to that used in the lattice QCD to study the quarkonium properties, which assumes a one-dimensional color flux tube structure. Because the flux tube structure may expand in more dimensions [66], it is better to consider the three-dimensional form of the medium-modified form of the Cornell potential, which we have done in this work.

C. Quark-antiquark potential in the anisotropic medium using the baryonic chemical potential

The spatial anisotropy (ξ) in noncentral heavy-ion collisions is generated at the early stages of QGP. As the system evolves with time, different pressure gradients are produced in different directions, which maps the spatial anisotropy to the momentum anisotropy. The anisotropy in this paper is introduced at the particle phase-space distribution level. Applying the method used in Refs. [36,39,68], the distribution function of anisotropy is obtained from the isotropic one by stretching and squeezing it in one of the directions in the momentum space as

$$f(\mathbf{p}) \rightarrow f_\xi(\mathbf{p}) = C_\xi f[\sqrt{\mathbf{p}^2 + \xi(\mathbf{p} \cdot \hat{\mathbf{n}})^2}], \quad (15)$$

where $f(\mathbf{p})$ represents the isotropic distribution function as in Refs. [35,59], and $\hat{\mathbf{n}}$ is the unit vector in the momentum anisotropy direction [for example, in squeezing ($\xi > 0$ or oblate case) and in stretching ($-1 < \xi < 0$ or prolate case) in the $\hat{\mathbf{n}}$ direction], whereas ξ denotes the anisotropy of the medium. Various EoS effects enter through the Debye screening mass (m_D). To make the Debye mass similar in both isotropic ($\xi = 0$) and anisotropic ($\xi \neq 0$) [36] media, we use the normalization constant C_ξ as follows:

$$C_\xi = \begin{cases} \frac{\sqrt{|\xi|}}{\tanh^{-1} \sqrt{|\xi|}} & \text{if } -1 \leq \xi < 0, \\ \frac{\sqrt{\xi}}{\tan^{-1} \sqrt{\xi}} & \text{if } \xi \geq 0. \end{cases} \quad (16)$$

If the limit of ξ is small, then we have

$$C_\xi = \begin{cases} 1 - \frac{\xi}{3} + O(\xi^{\frac{3}{2}}) & \text{if } -1 \leq \xi < 0, \\ 1 + \frac{\xi}{3} + O(\xi^{\frac{3}{2}}) & \text{if } \xi \geq 0. \end{cases} \quad (17)$$

In the presence of dissipative anisotropic hot QCD medium, we have modified the potential after considering the assumption given in Refs. [69–71]. The method to obtain the in-medium modification of the heavy-quark potential with the dielectric permittivity $\epsilon(k)$ has already been discussed in detail in Sec. II B. When modifying the potential, the foremost thing is to calculate the dielectric permittivity $\epsilon(\mathbf{k})$. To estimate the dielectric permittivity, there are two approaches: (i) with the help of gluon self-energy at finite-temperature QCD [72,73], and (ii) by the application of the semiclassical transport theory [39,74,75]. By exploiting either of these two methods, one can find the gluon self-energy tensor ($\Pi^{\mu\nu}$) and then the static gluon propagator represents inelastic scattering of an off-shell gluon to a thermal gluon:

$$\Delta^{\mu\nu}(\omega, \mathbf{k}) = k^2 g^{\mu\nu} - k^\mu k^\nu + \Pi^{\mu\nu}(\omega, \mathbf{k}), \quad (18)$$

where ω is the frequency, and the gluon self-energy tensor is symmetric and transverse in nature, i.e., $\Pi^{\mu\nu}(\omega, \mathbf{k}) =$

$\Pi^{\nu\mu}(\omega, \mathbf{k})$ and follows Ward's identity:

$$\Pi^{\mu\nu}(\omega, \mathbf{k}) = g^2 \int \frac{d^3 p}{(2\pi)^3} u^\mu \frac{\partial f(p)}{\partial p^\beta} \left[g^{\nu\beta} - \frac{u^\nu k^\beta}{uk + i\epsilon} \right]. \quad (19)$$

The term $\mu^\mu = (1 + \frac{\mathbf{k}}{|\mathbf{k}|})$ is a lightlike vector defining the propagation of plasma particles in space-time and in quantum chromodynamics plasma, whereas $f(p)$ is denoted as the arbitrary particle distribution function. In the Fourier space, gluon propagators with the real and imaginary parts of the potential obtained from the dielectric tensor of the temporal component, thus, become

$$\epsilon^{-1}(\mathbf{k}) = - \lim_{\omega \rightarrow 0} k^2 \Delta^{00}(\omega, \mathbf{k}), \quad (20)$$

where Δ^{00} represents the static limit of the 00 components of the gluon propagators in the Coulomb gauge. After performing the calculation (shown in the Appendix), we have calculated the real and imaginary parts of the temporal component of the propagator in the static limit using the quasiparticle Debye mass. The temporal component of the real part of the retarded propagator in the Fourier space, which is required to obtain the real part of the potential in the static limit [45], is given as

$$\text{Re}[\Delta_{R(A)}^{00}](\omega = 0, \mathbf{k}) = - \frac{1}{k^2 + m_D^2(T, \mu_b)} - \xi \left\{ \frac{1}{3[k^2 + m_D^2(T, \mu_b)]} - \frac{m_D^2(T, \mu_b)(3 \cos 2\theta_n - 1)}{6[k^2 + m_D^2(T, \mu_b)]^2} \right\}. \quad (21)$$

Similarly, the imaginary part can be derived from the imaginary part of the temporal component of the symmetric propagator [45], in the static limit, as follows:

$$\text{Im}[\Delta_S^{00}](\omega = 0, \mathbf{k}) + \frac{\pi T m_D^2}{k(k^2 + m_D^2)^2} = \pi T m_D^2 \xi \left[\frac{-1}{3k(k^2 + m_D^2)^2} + \frac{3 \sin^2 \theta_n}{4k(k^2 + m_D^2)^2} - \frac{2m_D^2(3 \sin^2 \theta_n - 1)}{3k(k^2 + m_D^2)^3} \right], \quad (22)$$

where

$$\cos(\theta_n) = \cos(\theta_r) \cos(\theta_{pr}) + \sin(\theta_r) \sin(\theta_{pr}) \cos(\phi_{pr}). \quad (23)$$

In the above expression, θ_n represents the angle between the particle momentum (\mathbf{p}) and the direction of anisotropy, θ_r denotes the angle between \mathbf{r} and \mathbf{n} . ϕ_{pr} and θ_{pr} are the azimuthal angle and the polar angle. Next, to modify the real part of the potential, $\epsilon(\mathbf{k})$ can be obtained using Eqs. (21) and (20) as

$$\epsilon^{-1}(\mathbf{k}) = \frac{k^2}{k^2 + m_D^2(T, \mu_b)} + k^2 \xi \times \left\{ \frac{1}{3[k^2 + m_D^2(T, \mu_b)]} - \frac{m_D^2(T, \mu_b)(3 \cos 2\theta_n - 1)}{6[k^2 + m_D^2(T, \mu_b)]^2} \right\}. \quad (24)$$

Similarly for the imaginary part, $\epsilon(\mathbf{k})$ can be obtained by employing Eq. (22) in Eq. (20) as

$$\epsilon^{-1}(\mathbf{k}) = \pi T m_D^2 \left[\frac{k^2}{k(k^2 + m_D^2)^2} - \xi k^2 \left(\frac{-1}{3k(k^2 + m_D^2)^2} + \frac{3 \sin^2 \theta_n}{4k(k^2 + m_D^2)^2} - \frac{2m_D^2[3 \sin^2(\theta_n) - 1]}{3k(k^2 + m_D^2)^3} \right) \right]. \quad (25)$$

The real and imaginary parts of the interquark potential can be obtained in the static limit using $\epsilon^{-1}(\mathbf{k})$, [35]. Using Eq. (24) in Eq. (12), we can write the real part of the potential as

$$\text{Re}[V(r, \theta_r, \xi, T, \mu_b)] = \int \frac{d^3 \mathbf{k}}{(2\pi)^{3/2}} (e^{i\mathbf{k}\cdot\mathbf{r}} - 1) \left(-\sqrt{\frac{2}{\pi}} \frac{\alpha}{k^2} - \frac{4\sigma}{\sqrt{2\pi}k^4} \right) \left[\frac{k^2}{k^2 + m_D^2} + k^2 \xi \left(\frac{1}{3(k^2 + m_D^2)} - \frac{m_D^2(3 \cos 2\theta_n - 1)}{6(k^2 + m_D^2)^2} \right) \right], \quad (26)$$

where $s = rm_D(T, \mu_b)$, and after considering the limit $s \ll 1$, the solution to the above integral yields

$$\text{Re}[V(r, \theta_r, \xi, T, \mu_b)] = \frac{s\sigma}{m_D} \left(1 + \frac{\xi}{3} \right) - \frac{\alpha m_D}{s} \left\{ 1 + \frac{s^2}{2} + \xi \left[\frac{1}{3} + \frac{s^2}{16} \left(\frac{1}{3} + \cos(2\theta_r) \right) \right] \right\}. \quad (27)$$

The imaginary potential using Eq. (25) in Eq. (12) is

$$\begin{aligned} \text{Im}[V(r, \theta_r, \xi, T, \mu_b)] &= \pi T m_D^2(T, \mu_b) \int \frac{d^3 \mathbf{k}}{(2\pi)^{3/2}} (e^{i\mathbf{k}\cdot\mathbf{r}} - 1) \left(-\sqrt{\frac{2}{\pi}} \frac{\alpha}{k^2} - \frac{4\sigma}{\sqrt{2\pi}k^4} \right) \left(\frac{k}{[k^2 + m_D^2(T, \mu_b)]^2} \right) \\ &\quad - \pi T m_D^2(T, \mu_b) \xi \int \frac{d^3 \mathbf{k}}{(2\pi)^{3/2}} (e^{i\mathbf{k}\cdot\mathbf{r}} - 1) \\ &\quad \times \left(-\sqrt{\frac{2}{\pi}} \frac{\alpha}{k^2} - \frac{4\sigma}{\sqrt{2\pi}k^4} \right) \left(\frac{-k}{3[k^2 + m_D^2(T, \mu_b)]^2} + \frac{3k \sin^2 \theta_n}{4[k^2 + m_D^2(T, \mu_b)]^2} \right. \\ &\quad \left. - \frac{2m_D^2(T, \mu_b)k(3 \sin^2 \theta_n - 1)}{[k^2 + m_D^2(T, \mu_b)]^2} \right). \end{aligned} \quad (28)$$

Up to the leading logarithmic order, the imaginary potential is

$$\begin{aligned} \text{Im}[V(r, \theta_r, T, \mu_b, \xi)] &= \frac{\alpha s^2 T}{3} \left\{ \frac{\xi}{60} (7 - 9 \cos 2\theta_r) - 1 \right\} \log \frac{1}{s} \\ &\quad + \frac{s^4 \sigma T}{m_D^2(T, \mu_b)} \left\{ \frac{\xi}{35} \left(\frac{1}{9} - \frac{1}{4} \cos 2\theta_r \right) - \frac{1}{30} \right\} \log \frac{1}{s}. \end{aligned} \quad (29)$$

Figures 1 and 2 show the variation of the real and imaginary potential with distance (r) at a constant temperature of $T = 300$ MeV. Figures 1(a) and 2(a) show the real and imaginary parts of the potential for different anisotropic cases: prolate $\xi = -0.3$, oblate $\xi = 0.3$, and isotropic $\xi = 0$ at $\mu_b = 300$ MeV and $\theta = 0^\circ$ (parallel case) and $\theta = 90^\circ$ (perpendicular case). An increase in the real potential is observed as one goes from the prolate case to the oblate case. The imaginary potential decreases from the prolate case to the oblate case in the parallel case but increases for the perpendicular case. Figures 1(b) and 2(b) represent the same variation for real and imaginary potentials at constant $\xi = 0.3$ for different values of $\mu_b = 300, 1000$, and 2000 MeV. It was observed that the real potential increases with r for different baryonic chemical potentials, and the imaginary potential shows a decreasing pattern. In short, potentials (real and imaginary) have higher

values for perpendicular cases [Figs. 1(b) and 2(b)]. This indicates that anisotropy and the baryonic chemical potential have a significant effect on complex valued potentials.

III. CALCULATIONS AND RESULTS

A. Binding energy (B.E.) of the different quarkonium S states

Now using Refs. [43,45,76], the binding energies of heavy-quarkonium states in the anisotropic medium can be obtained by solving the Schrödinger equation with the first-order perturbation in the anisotropy parameter (ξ). The expression of the real part of the binding energy is as follows:

$$\begin{aligned} \text{Re}[\text{B.E.}] &= \frac{m_Q \sigma^2}{m_D^4(T, \mu_b) n^2} + \alpha m_D(T, \mu_b) \\ &\quad + \frac{\xi}{3} \left(\frac{m_Q \sigma^2}{m_D^4(T, \mu_b) n^2} + \alpha m_D(T, \mu_b) \right. \\ &\quad \left. + \frac{2m_Q \sigma^2}{m_D^4(T, \mu_b) n^2} \right), \end{aligned} \quad (30)$$

Where $n = 1$ and $n = 2$ correspond to the ground and first excited states of the heavy quarkonia, respectively. It should be noted here that the above expression of the binding energy [Eq. (30)] is applicable only for J/ψ , Υ , Ψ' , and Υ' .

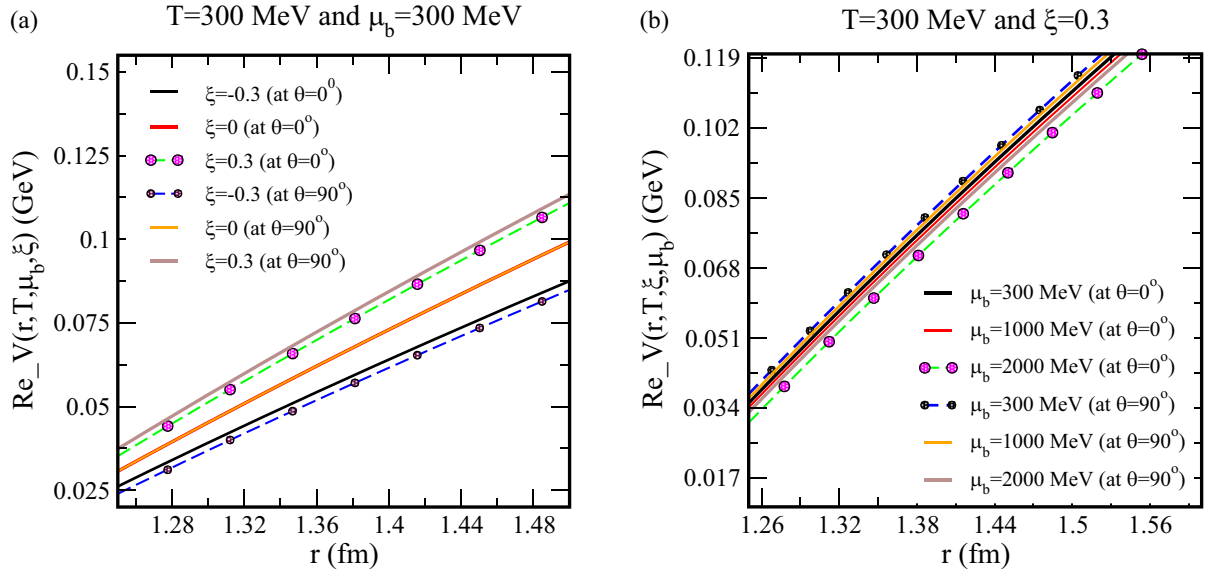


FIG. 1. Variation of the real potential with distance (r in Fermi) at different values of anisotropy (a) and at different values of the baryonic chemical potential (b) in both the parallel case and the perpendicular case.

Figures 3 and 4 show variation of the binding energy of J/ψ , Υ , ψ' , and Υ' with T/T_c at different values of the baryonic chemical potential (μ_b) (i.e., $\mu_b = 200, 1000$, and 2000 MeV) and at a constant value of anisotropy (ξ) (i.e., $\xi = 0.3$). From Figures 3 and 4 it can be deduced that the binding energy of J/ψ , Υ , ψ' , and Υ' decreases if the value of μ_b is increased. Figures 5 and 6 show variation of the binding energy of J/ψ , Υ , ψ' , and Υ' with T/T_c at different values of anisotropy (ξ) (i.e., $\xi = 0.3, 0$, and -0.3) and at a constant value of μ_b (i.e., $\mu_b = 1000$ MeV). Figures 5 and 6 show that the binding energy of J/ψ , Υ , ψ' , and Υ'

increases if the value of ξ is increased. It is noticed from the present calculations that the binding energy has higher values as one moves from the prolate case ($\xi < 0$) to the oblate case ($\xi > 0$). In an anisotropic medium, the binding energy of the $Q\bar{Q}$ pair gets stronger with an increase in anisotropy. This is due to the fact that the variation of the binding energy increases if we go from the prolate case to the oblate case, and hence quarkonium states are strongly bound with anisotropy. With the help of binding energy expression we have also calculated the mass spectra of quarkonium state shown by the Figs. 7 and 8.

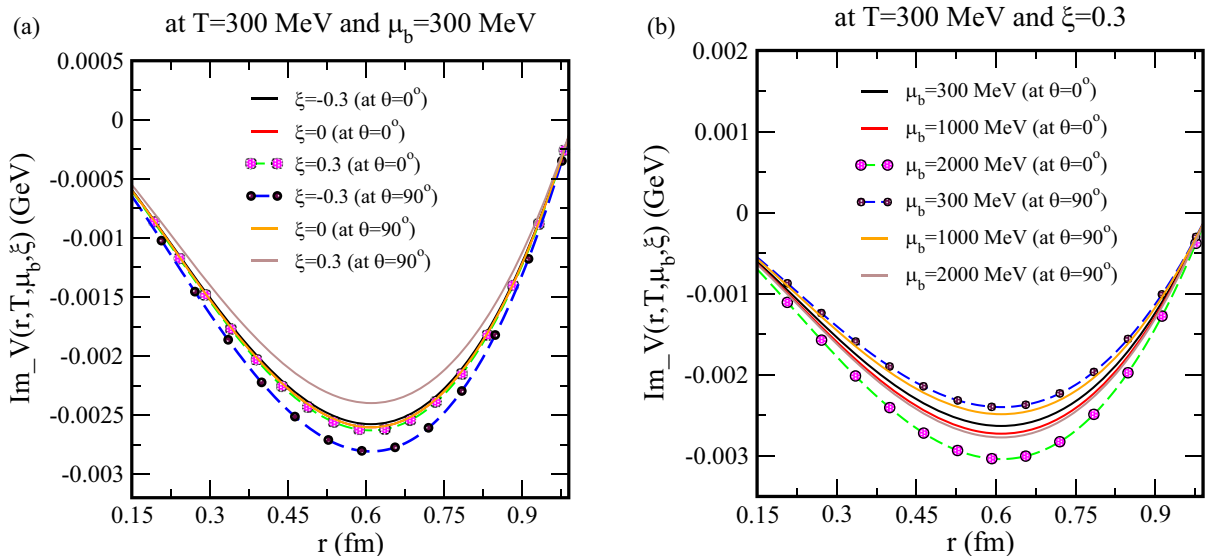


FIG. 2. Variation of the imaginary potential with distance (r in Fermi) at different values of anisotropy (a) and at different values of the baryonic chemical potential (b) in both the parallel case and the perpendicular case.

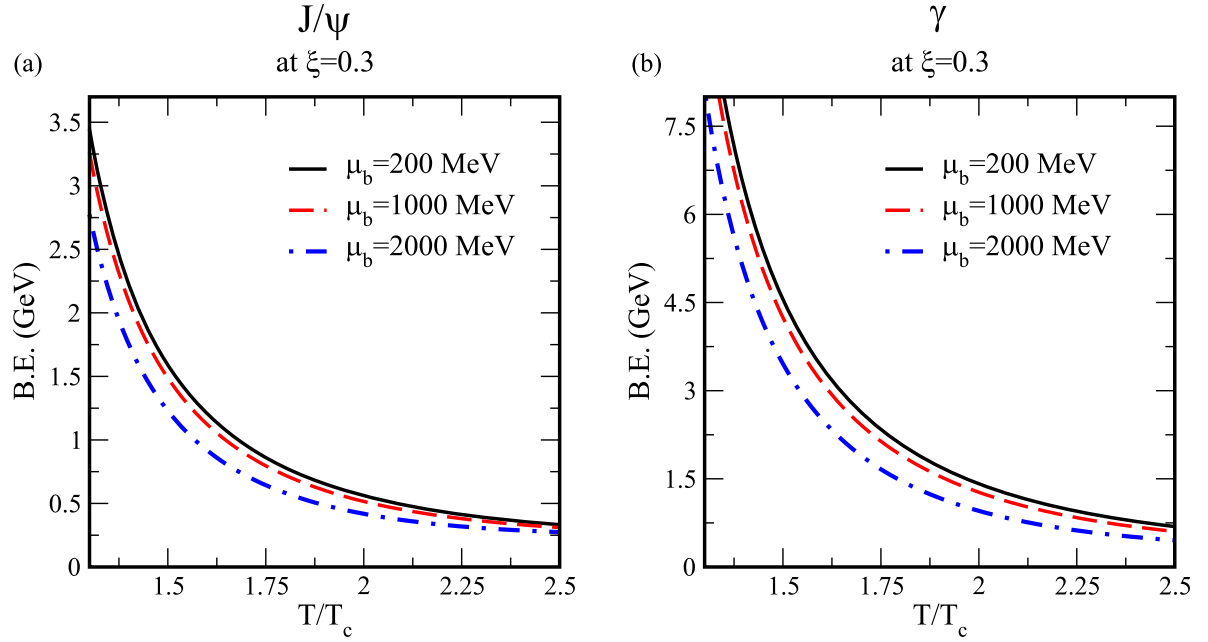


FIG. 3. Variation of the binding energy of J/ψ (a) and Υ (b) with T/T_c at different values of the baryonic chemical potential (μ_b) when the value of ξ is fixed.

B. Dissociation of quarkonium states in the presence of ξ and the baryonic chemical potential

The dissociation temperature for real binding energies can be obtained by using the thermal energy effect. According to Refs. [46,77], it is not necessary to have zero binding energy for dissolution of the quarkonium states. When the binding energy ($B.E. \leq T$) of the quarkonium state is weakly bonded,

the quarkonium state dissociates by means of thermal fluctuations. The quarkonium state is also said to be dissociated when $2B.E. < \Gamma(T)$, where $\Gamma(T)$ is the thermal width of the respective quarkonium states. When the binding energy of charmonium and bottomonium states at a particular value of temperature becomes smaller or equal to the value of the mean thermal energy, the state is said to be dissociated and this can be estimated by using the expressions $B.E. = T_D$ (for

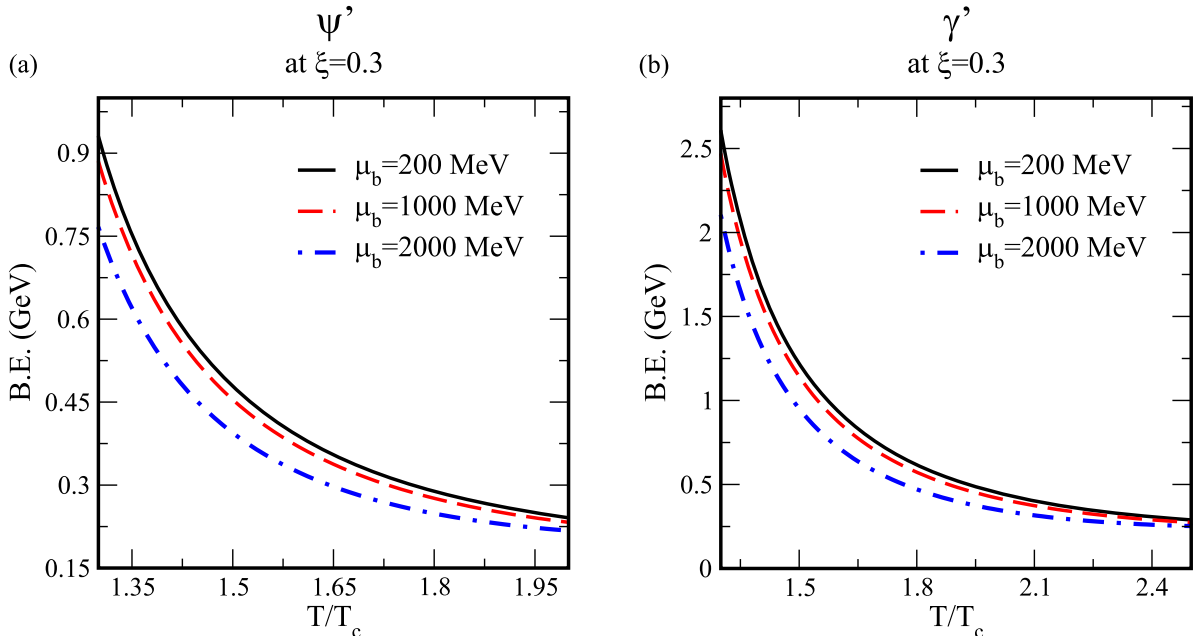


FIG. 4. Variation of the binding energy of ψ' (a) and Υ' (b) with T/T_c at different values of the baryonic chemical potential (μ_b) where the value of ξ is fixed.

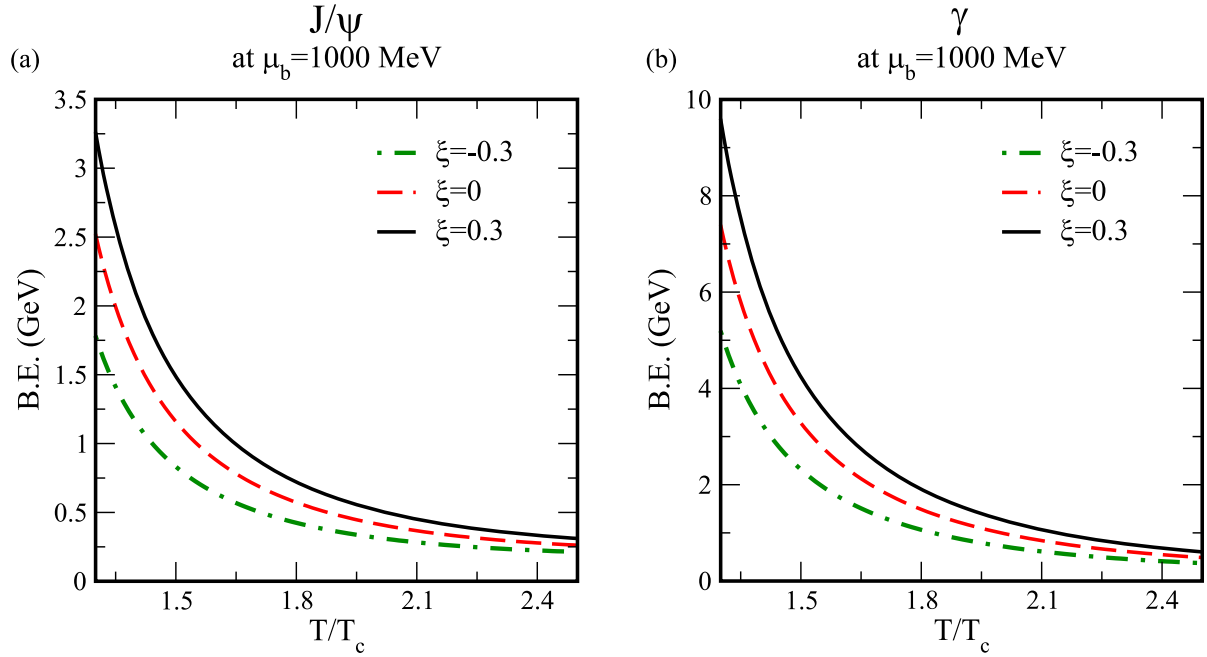


FIG. 5. Variation of the binding energy of J/ψ (a) and γ (b) with T/T_c at different values of anisotropy (ξ) and when the value of μ_b is fixed.

the upper bound of quarkonium dissociation) and $B.E. = 3T_D$ (for the lower bound of quarkonium dissociation), as can be found in Ref. [78] and references therein, and is written as follows:

$$B.E._{(J/\psi, \gamma, \psi', \gamma')}$$

$$= \frac{m_Q \sigma^2}{m_D^4(T, \mu_b) n^2} + \alpha m_D(T, \mu_b)$$

$$+ \frac{\xi}{3} \left(\frac{m_Q \sigma^2}{m_D^4(T, \mu_b) n^2} + \alpha m_D(T, \mu_b) + \frac{2m_Q \sigma^2}{m_D^4(T, \mu_b) n^2} \right)$$

$$= \begin{cases} T_D & \text{for upper bound,} \\ 3T_D & \text{for lower bound.} \end{cases} \quad (31)$$

Further, we have calculated the dissociation temperature by using two criteria: first by using the mean thermal

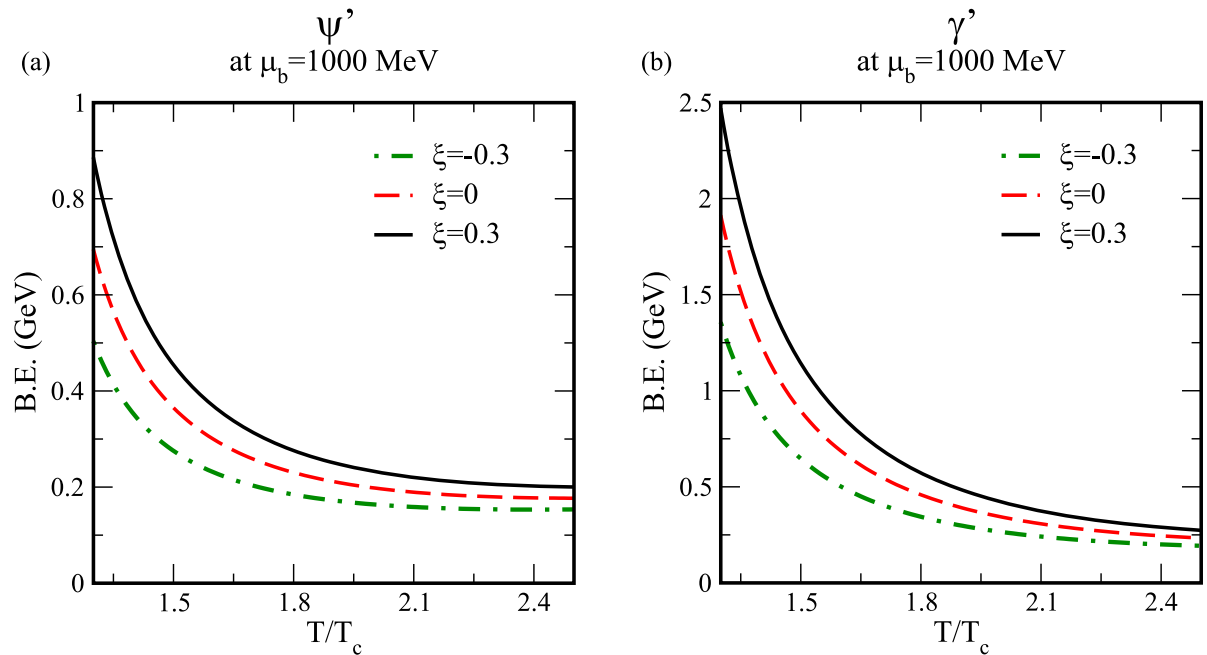


FIG. 6. Variation of the binding energy of ψ' (a) and γ' (b) with T/T_c at different values of anisotropy (ξ) where the value of μ_b is fixed.

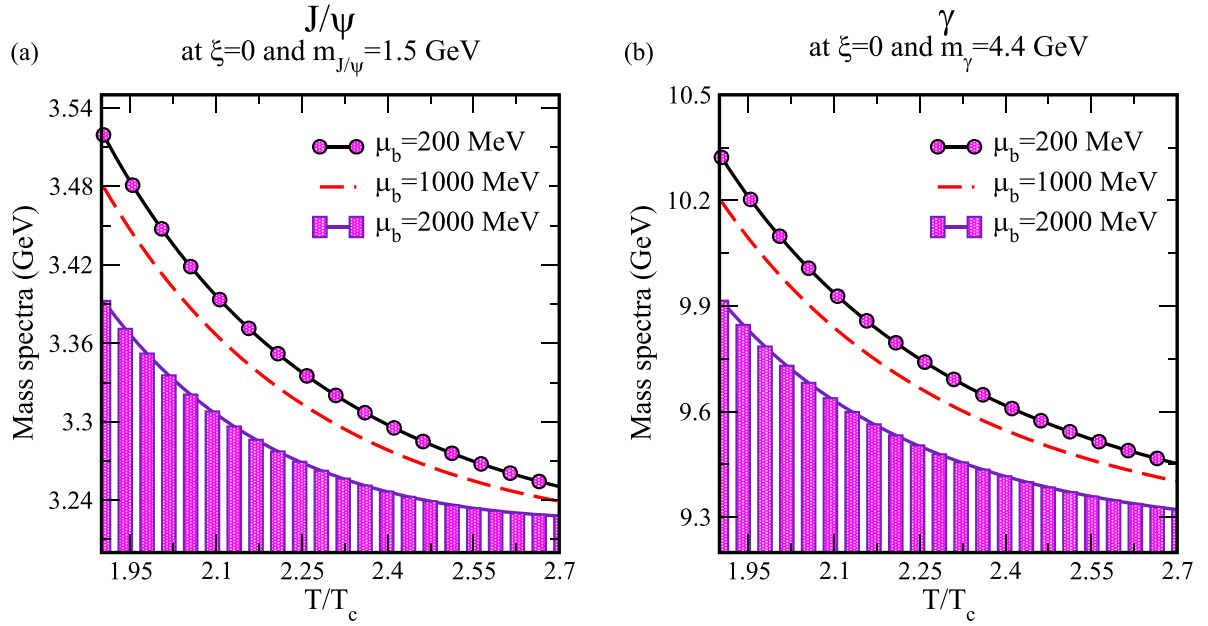


FIG. 7. Variation of mass spectra of J/ψ (a) and Υ (b) with T/T_c at different values of anisotropy (ξ) when the value of μ_b is fixed.

energy and second by using the thermal width. The dissociation temperatures of quarkonium states by using the mean thermal energy effect criteria are listed in Tables I–IV for both lower and upper bounds. In general, the dissociation temperature decreases with an increase in the values of μ_b (i.e., $\mu_b = 200, 1000,$ and 2000 MeV) and increases with an increase in the values of ξ (i.e., $\xi = -0.3, 0,$ and 0.3).

C. Thermal width of S states of quarkonium

As already mentioned in Sec. II(c), the quarkonium potential has both real and imaginary parts. The real part gives rise

to the binding energy as discussed earlier, whereas the thermal width comes from the imaginary part of the potential. The thermal width is now employed to calculate the dissociation point by exploiting twice the real binding energy with the thermal width of the quarkonium states. Thus, the thermal width can be obtained as

$$\Gamma(T) = - \int d^3\mathbf{r} |\Psi(r)|^2 \text{Im} V(\mathbf{r}), \quad (32)$$

where $\Psi(r)$ is the Coulombic-type wave function. The Coulombic wave functions for J/ψ , Υ , ψ' , and Υ' are given

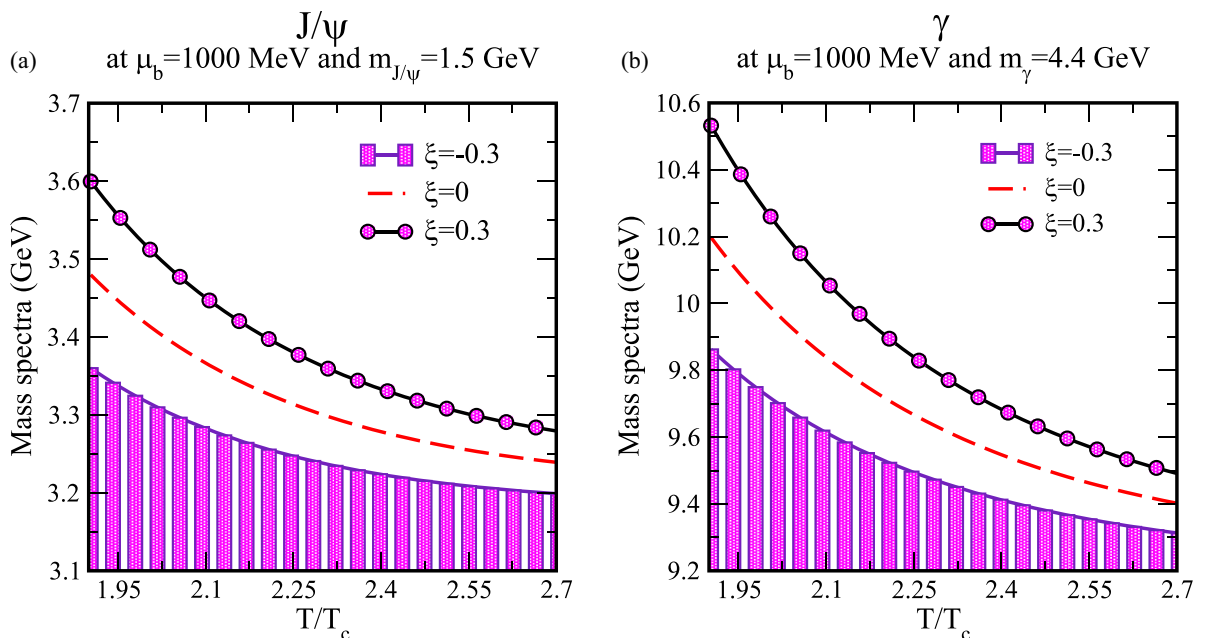


FIG. 8. Variation of mass spectra of J/ψ (a) and Υ (b) with T/T_c at different values of anisotropy (ξ) where the value of μ_b is fixed.

TABLE I. Lower bound of dissociation for $\xi = 0.3$ at $T_c = 197$ MeV. Temperatures are given in units of T_c .

States	Dissociation by thermal energy effect criteria		
	$\mu_b = 200$ MeV	$\mu_b = 1000$ MeV	$\mu_b = 2000$ MeV
J/ψ	1.6497	1.6243	1.5736
Υ	2.0558	2.0050	1.8908
Υ'	1.6143	1.5931	1.5285

as

$$\begin{aligned}\Psi_{1S}(r) &= \frac{1}{\sqrt{\pi a_0^3}} e^{-\frac{r}{a_0}}, \\ \Psi_{2S}(r) &= \frac{1}{4\sqrt{2\pi a_0^3}} \left(2 - \frac{r}{a_0}\right) e^{-\frac{r}{2a_0}},\end{aligned}\quad (33)$$

where $a_0 = 2/(m_Q\alpha)$ represents the Bohr radius of the quarkonium system. Now by using Eq. (33), we have

$$\begin{aligned}\Gamma_{1S/2S}(T) &= m_D^2 \text{Tr}^2 \log \left(\frac{1}{rm_D} \right) \int d^3r |\Psi_{1s/2s}(r)|^2 \\ &\times \left\{ \frac{\alpha}{3} \left[\frac{\xi}{60} (7 - 9 \cos 2\theta_r) - 1 \right] \right\} \\ &+ m_D^2 \text{Tr}^2 \log \left(\frac{1}{rm_D} \right) \int d^3r |\Psi_{1s/2s}(r)|^2 \\ &\times \left\{ \sigma r^2 \left[\frac{\xi}{35} \left(\frac{1}{9} - \frac{1}{4} \cos 2\theta_r \right) - \frac{1}{30} \right] \right\}.\end{aligned}\quad (34)$$

The thermal width for the 1S state can be obtained by solving the above equation as follows:

$$\begin{aligned}\Gamma_{1S}(T) &= \frac{m_D^2 T (\xi - 6)}{90\alpha^4 m_Q^4} \\ &\times [5(12\gamma - 25)\alpha^3 m_Q^2 + 9(20\gamma - 49)\sigma] \\ &= \frac{m_D^2 T (\xi - 6)}{90\alpha^4 m_Q^4} \left[60(\alpha^3 m_Q^2 + 3\sigma) \log \left(\frac{\alpha M_Q}{m_D} \right) \right].\end{aligned}\quad (35)$$

Thus, the dissociation width for the 1S state up to the leading logarithmic order of the imaginary potential following

TABLE II. Upper bound of dissociation for $\xi = 0.3$ at $T_c = 197$ MeV. Temperatures are in units of T_c .

States	Dissociation by thermal energy effect criteria		
	$\mu_b = 200$ MeV	$\mu_b = 1000$ MeV	$\mu_b = 2000$ MeV
J/ψ	2.0812	2.0304	1.9162
Υ	2.6142	2.5253	2.3350
Υ'	2.0431	1.9162	1.7893

TABLE III. Lower bound of dissociation for $\mu_b = 1000$ MeV at $T_c = 197$ MeV. Temperatures are in units of T_c .

States	Dissociation by thermal energy effect criteria		
	$\xi = -0.3$	$\xi = 0$	$\xi = 0.3$
J/ψ	1.4593	1.5482	1.6243
Υ	1.7766	1.9035	2.0050
Υ'	1.4086	1.5355	1.5931

Ref. [45] would be of the form

$$\frac{\Gamma_{1S}(T)}{m_D^2 \log \left(\frac{m_Q}{\alpha m_Q} \right)} = T \left(\frac{4}{\alpha m_Q^2} + \frac{12\sigma}{\alpha^4 m_Q^4} \right) \left(1 - \frac{\xi}{6} \right).\quad (36)$$

Similarly for the 2S state, using the wave function for the 2S state, we have

$$\begin{aligned}\Gamma_{2S}(T) &= \frac{T(\xi - 6)}{45\alpha^2 m_Q^2} m_D^2 \left(35(12\gamma - 31)\alpha + \frac{72(160\gamma - 447)\sigma}{\alpha^2 m_Q^2} \right) \\ &+ \frac{T(\xi - 6)}{45\alpha^2 m_Q^2} m_D^2 \left\{ 60 \left(7\alpha + \frac{192\sigma}{\alpha^2 m_Q^2} \right) \log \left(\frac{\alpha m_Q}{2m_D} \right) \right\}.\end{aligned}\quad (37)$$

The leading logarithmic order for the 2S state is given as

$$\frac{\Gamma_{2S}(T)}{\log \left(\frac{2m_D}{\alpha m_Q} \right)} = \frac{8m_D^2 T}{\alpha^4 m_Q^4} \left(1 - \frac{\xi}{6} \right) (7\alpha^3 m_Q^2 + 192\sigma).\quad (38)$$

The dissociation temperatures of different quarkonium states obtained by exploiting the thermal width and twice the real binding energy are shown in the Fig. 9 (for J/ψ), Fig. 10 (for Υ), and Fig. 11 (for Υ'). The dissociation temperatures obtained from the intersection point of twice the real binding energy and the thermal width for different states at different values of anisotropy (ξ) and the baryonic chemical potential are listed in Tables V and VI. There were no dissociation temperatures found for ψ' due to its small mass value and hence it decays earlier than the ground state.

D. Mass spectra of quarkonium states in the presence of anisotropy and the baryonic chemical potential

The mass spectra of 1S and 2S states of charmonium and bottomonium in the anisotropic medium can be calculated by

TABLE IV. Upper bound of dissociation for $\mu_b = 1000$ MeV at $T_c = 197$ MeV. Temperatures are in units of T_c .

States	Dissociation by thermal energy effect criteria		
	$\xi = -0.3$	$\xi = 0$	$\xi = 0.3$
J/ψ	1.7766	1.9162	2.0304
Υ	2.2081	2.3730	2.5253
Υ'	1.7893	1.8821	1.9162

TABLE V. Dissociation for $\mu_b = 1000$ MeV at $T_c = 197$ MeV. Temperatures are in units of T_c .

States	Dissociation by thermal width criteria		
	$\xi = -0.3$	$\xi = 0$	$\xi = 0.3$
J/ψ	1.3879	1.4202	1.4467
Υ	2.8232	2.8857	2.9409
Υ'	1.5644	1.5788	1.5909

using the following condition:

$$M = 2m_Q + B.E. \quad (39)$$

Hence, we have

mass spectra of quarkonium states

$$= 2m_Q + \left[\frac{m_Q \sigma^2}{m_D^4 n^2} + \alpha m_D + \frac{\xi}{3} \left(\frac{m_Q \sigma^2}{m_D^4 n^2} + \alpha m_D + \frac{2m_Q \sigma^2}{m_D^4 n^2} \right) \right], \quad (40)$$

where m_Q is the mass of heavy quarkonia.

Figures 7 and 8 show the variation of mass spectra of J/ψ [panel (a)] and Υ [panel (b)] with T/T_c at different values of baryonic chemical potential (μ_b) (i.e., $\mu_b = 200, 1000,$ and 2000 MeV) (in Fig. 7) and at different values of ξ (i.e., $\xi = -0.3, 0,$ and 0.3) (in Fig. 8). From Figs. 7 and 8 it can be observed that the values of mass spectra of J/ψ and Υ decrease if we increase the value of μ_b and increase if we increase the value of ξ . In Tables VII and VIII, we have calculated the values of mass spectra. Table VII shows that the values of mass spectra decrease with increases in μ_b . Further from Table VIII, it can be seen that the values of mass spectra increase with ξ . We have also compared the results of mass spectra at different values of μ_b (in Table VII) and at different

TABLE VI. Dissociation for $\xi = 0.3$ at $T_c = 197$ MeV. Temperatures are in units of T_c .

States	Dissociation by thermal width criteria		
	$\mu_b = 200$ MeV	$\mu_b = 1000$ MeV	$\mu_b = 2000$ MeV
J/ψ	1.4618	1.4467	1.4082
Υ	3.0775	2.9385	2.6794
Υ'	1.6127	1.5913	1.5379

values of ξ (in Table VIII) with the previously published theoretical [38] and experimental [79] results. The presently calculated values of mass spectra are found to be in agreement with the experimental and theoretical values reported earlier [38,79].

E. Thermodynamical properties of quark matter with the anisotropic parameter (ξ) obtained using EoSs of QGP

The EoSs played an invaluable role in understanding the behavior of QGP that is produced in relativistic nucleus-nucleus collisions. EoSs are very sensitive to matter and are important to verify and investigate the suppression of quarkonia [80,81]. The expansion of QGP is highly sensitive to EoSs via the speed of sound, and it investigates the sensitivity of quarkonium suppression to the EoS [80,81]. Bannur [83] created an EoS for a strongly coupled QGP by appropriate modification of strongly coupled plasma in QED by integrating the running coupling constant and making suitable adjustments to account for color and flavor degree of freedom and found a pretty good fit to the lattice findings. Now, we have gone through the EoSs, which are stated as a function of

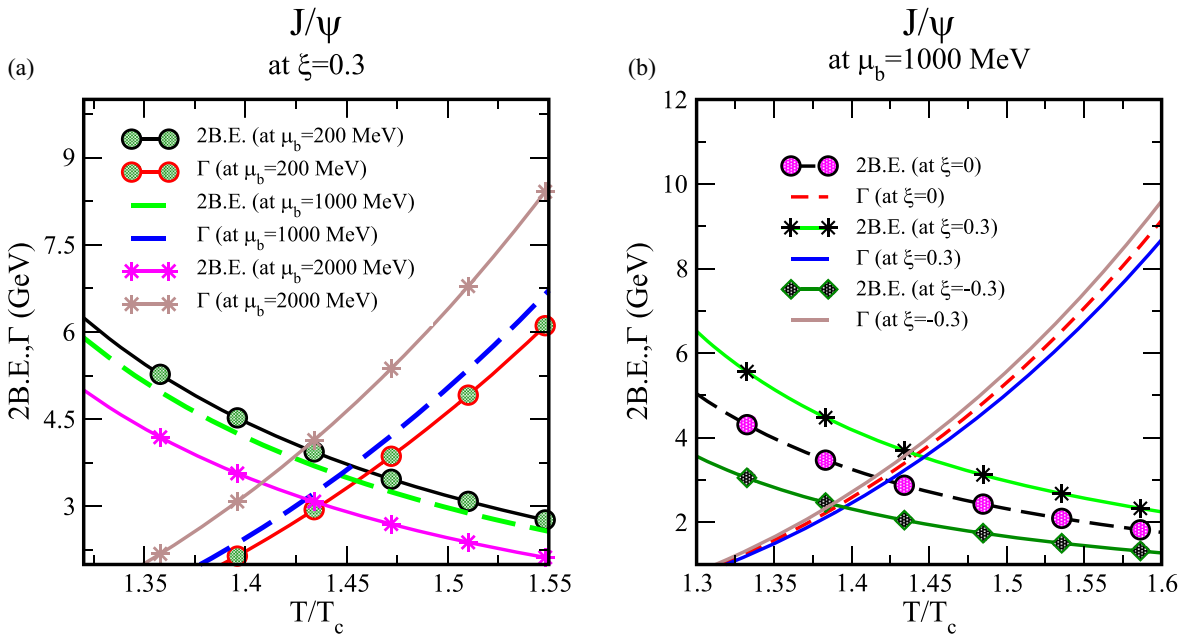


FIG. 9. Variation of 2B.E. and Γ of J/ψ with T/T_c at different values of μ_b (a) and at different values of ξ (b).

TABLE VII. Mass spectra of ground state of quarkonium at $\xi = 0$. Mass spectra are in units of GeV.

States	For $m_{J/\psi} = 1.5$ GeV and $m_\Upsilon = 4.5$ GeV			Theoretical result [38]	Experimental result [79]
	$\mu_b = 200$ MeV	$\mu_b = 1000$ MeV	$\mu_b = 2000$ MeV		
J/ψ	3.520	3.480	3.391	3.060	3.096
Υ	10.32	10.18	9.909	9.200	9.460

the plasma parameter [84], briefly:

$$\epsilon_{\text{QED}} - nT \mu_{\text{ex}}(\Gamma) = \frac{3}{2} nT. \quad (41)$$

The first term represents the ideal contribution, and the deviation from the ideal EoS is as follows:

$$\begin{aligned} & \mu_{\text{ex}}(\Gamma)(1 + 3 \times 10^3 \Gamma^{5.7}) \\ &= \mu_{\text{ex}}^{\text{Abe}}(\Gamma) + 3 \times 10^3 \Gamma^{5.7} \mu_{\text{ex}}^{\text{OCP}}(\Gamma), \end{aligned} \quad (42)$$

where $\mu_{\text{ex}}^{\text{Abe}}$ is

$$\mu_{\text{ex}}^{\text{Abe}} + 3\Gamma^3 \left[\frac{3}{8} \ln(3\Gamma) + \frac{\gamma}{2} - \frac{1}{3} \right] = -\frac{\sqrt{3}}{2} \Gamma^{\frac{3}{2}}, \quad (43)$$

where the term $\mu_{\text{ex}}^{\text{Abe}}$ is determined for the plasma component and is valid for all $\Gamma < 180$ [85], and the term $\mu_{\text{ex}}^{\text{OCP}}$ is

$$\begin{aligned} & \mu_{\text{ex}}^{\text{OCP}} - (0.220703\Gamma^{-\frac{1}{4}} - 0.86097) \\ &= -0.898004\Gamma + 0.96786\Gamma^{\frac{1}{4}}. \end{aligned} \quad (44)$$

For strongly coupled plasma, in QCD it was assumed that the hadron exists for $T < T_c$ and goes to QGP for $T > T_c$. At $T > T_c$, it is the strongly interacting plasma of quarks, gluons, and no hadrons, because it is assumed that the interaction of confinement due to the QCD vacuum has been melted [83] at $T = T_c$. Hence, only the Coulomb interaction is present in the deconfined plasma phase. So, the plasma parameter, which is the ratio of the particle average potential energy to the particle average kinetic energy, is assumed to be weak, $\Gamma \ll 1$, and is given by

$$\Gamma \equiv \frac{\langle PE \rangle}{\langle KE \rangle} = \frac{\text{Re}[V(r, T)]}{T}. \quad (45)$$

Finally, the EoS has been obtained by using the potential Eq. (8) in the plasma parameter after the inclusion of quantum and relativistic effects as

$$\frac{\epsilon_s}{nT} = [3 + \mu_{\text{ex}}(\Gamma)], \quad (46)$$

TABLE VIII. Mass spectra of ground state of quarkonium at $\mu_b = 1000$ MeV. Mass spectra are in units of GeV.

States	For $m_{J/\psi} = 1.5$ GeV and $m_\Upsilon = 4.5$ GeV			Theoretical result [38]	Experimental result [79]
	$\xi = -0.3$	$\xi = 0$	$\xi = 0.3$		
J/ψ	3.361	3.480	3.597	3.060	3.096
Υ	9.864	10.18	10.53	9.200	9.460

where μ_{ex} remains the same as in Eq. (42). The scaled energy density is now expressed in terms of the ideal contribution:

$$e(\Gamma) \equiv \frac{\epsilon_s}{\epsilon_{\text{SB}}} = 1 + \frac{1}{3} \mu_{\text{ex}}(\Gamma), \quad (47)$$

$$\epsilon_{\text{SB}} \equiv (16 + 21N_f/2)\pi^2 T^4/30. \quad (48)$$

Here, N_f denotes the number of quark and gluon flavors. For the $\overline{\text{MS}}$ approach, we now use two-loop-level QCD running coupling constants [86]:

$$g^2(T) \approx 2b_0 \ln \frac{\bar{\mu}}{\Lambda_{\overline{\text{MS}}}} \left(1 + \frac{b_1}{2b_0^2} \frac{\ln(2 \ln \frac{\bar{\mu}}{\Lambda_{\overline{\text{MS}}})}{\ln \frac{\bar{\mu}}{\Lambda_{\overline{\text{MS}}}}} \right)^{-1}, \quad (49)$$

where $b_0 = \frac{33-2N_f}{48\pi^2}$ and $b_1 = \frac{153-19N_f}{384\pi^4}$. In the case of the $\overline{\text{MS}}$ scheme, $\Lambda_{\overline{\text{MS}}}$ and $\bar{\mu}$ are considered as the renormalization scale and the scale parameter, respectively,

$$\bar{\mu} \exp(\gamma_E + c) = \Lambda_{\overline{\text{MS}}}(T),$$

$$\Lambda_{\overline{\text{MS}}}(T) \exp(\gamma_E + c) = 4\pi \Lambda_T. \quad (50)$$

Here, $\gamma_E = 0.5772156$ and $c = \frac{N_c - 4N_f \ln 4}{22N_c - N_f}$, which is a constant depending on colors and flavors. There are various uncertainties in the formula for the running coupling constant, which are connected with the scale parameter and the renormalization scale $\overline{\text{MS}}$. This problem has been superseded by using Brodsky-Lepage-Mackenzie criterion [87]. $\overline{\text{MS}}$ was permitted to fluctuate between πT and $4\pi T$ [88]. For our motivation, we chose $\overline{\text{MS}}$ near to the center value $2\pi T_c$ [77] for $N_f = 0$ and near to T_c for both $N_f = 2$ and $N_f = 3$ flavors.

When the factor $\frac{b_1}{2b_0^2} \frac{\ln(2 \ln \frac{\bar{\mu}}{\Lambda_{\overline{\text{MS}}})}{\ln \frac{\bar{\mu}}{\Lambda_{\overline{\text{MS}}}}}$ is $\gg 1$, then the expression is reduced as used in Ref. [83], ignoring the higher-order terms of the preceding component. However, this option does not hold true for the temperature ranges employed in the computation, resulting in a coupling mistake that ultimately causes the difference in findings between our model and the Bannur model [83]. First, we have computed the energy density $\epsilon_s(T)$ using Eq. (47) and the thermodynamic relation

$$\epsilon_s + P = T \frac{dp}{dT}. \quad (51)$$

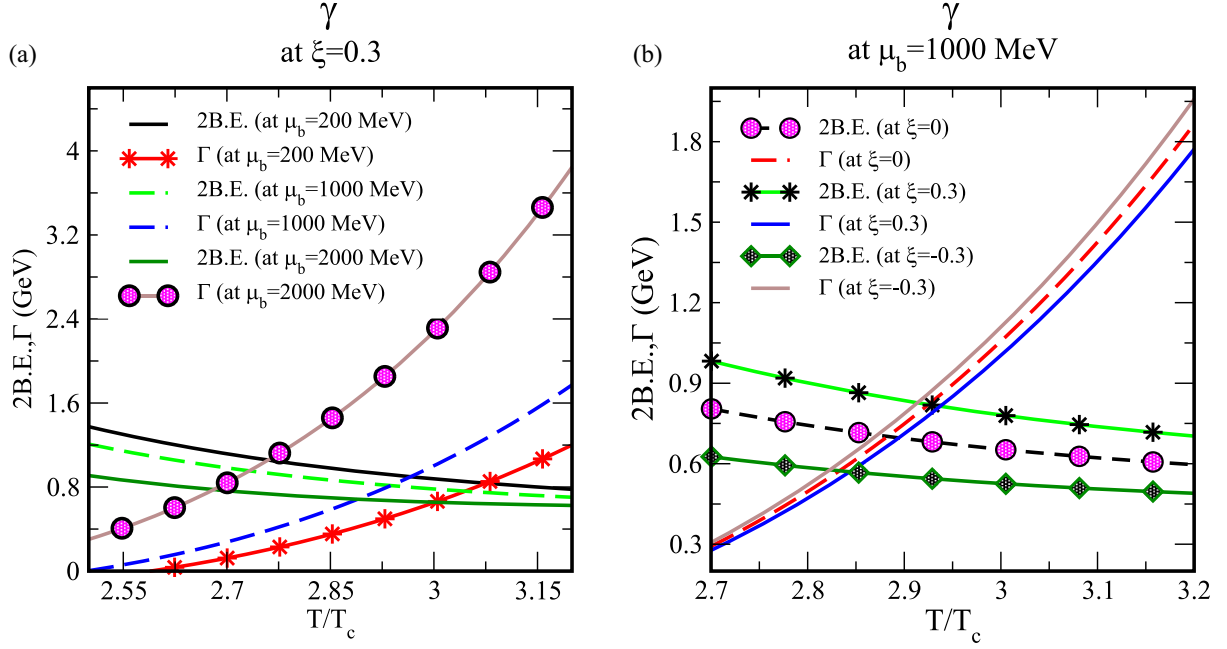


FIG. 10. Variation of 2B.E. and Γ of Υ with T/T_c at different values of μ_b (a) and at different values of ξ (b).

Further, the pressure was calculated as

$$\frac{P}{T^4} = \left(\frac{P_0}{T_0} + 3a_f \int_{T_0}^T d\tau \tau^2 e(\Gamma(\tau)) \right) / T^3. \quad (52)$$

Here, P_0 denotes the pressure at some temperature T_0 and $a_f = (16 + \frac{21}{2}N_f)\frac{\pi^2}{90}T^4$. Thus, the speed of sound can be evaluated once we have pressure (P) and the energy density (ϵ_s) in hand and is given as

$$c_s^2 d\epsilon_s = dP. \quad (53)$$

All the above thermodynamical properties are potential dependent, and the potential is Debye mass dependent. In that case, we attack the problem by trading off the dependence on the baryonic chemical potential (μ_b), the anisotropy (ξ), and the temperature to a dependence on these thermodynamic properties of matter. The thermodynamical properties of quark matter (i.e., pressure, energy density, and speed of sound) play a curious role in the study of QGP and also provide useful information about the strange quark matter. The thermodynamic behavior of QCD matter at high temperature or above critical

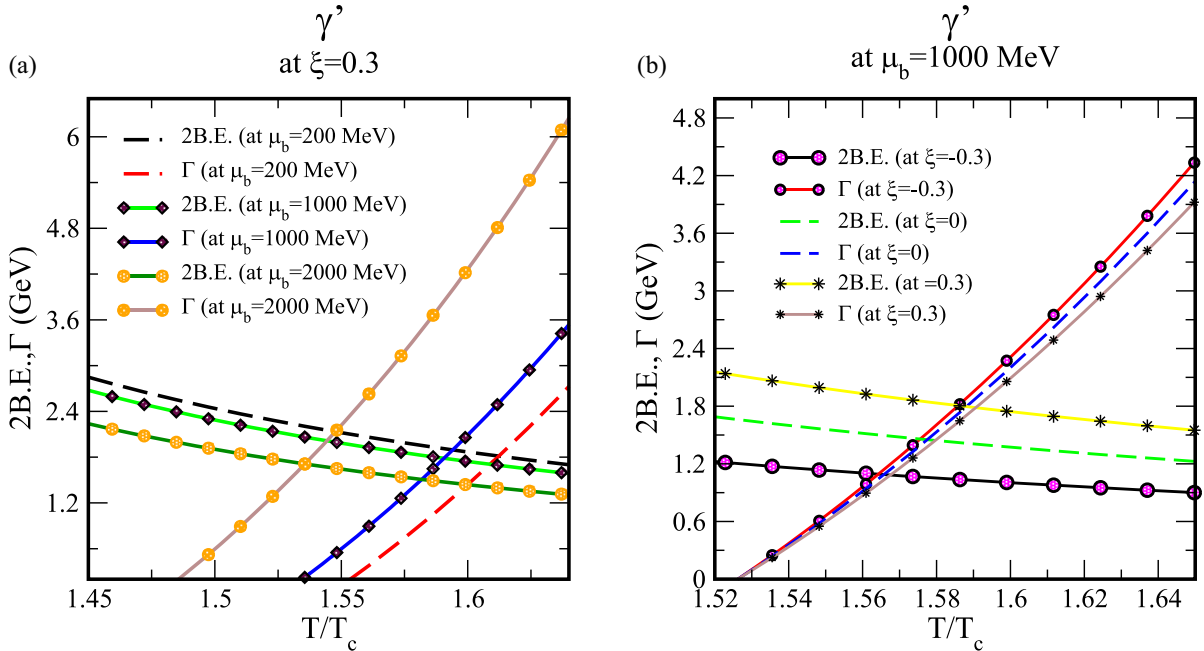


FIG. 11. Variation of 2B.E. and Γ of Υ' with T/T_c at different values of μ_b (a) and at different values of ξ (b).

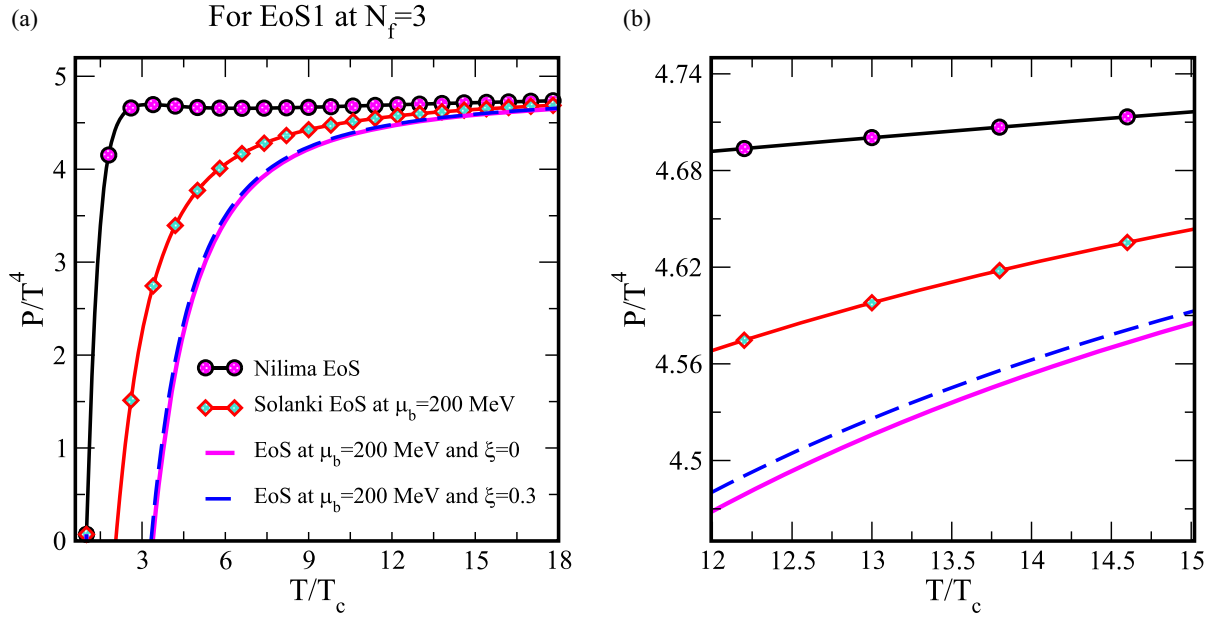


FIG. 12. (a) Variation of P/T^4 with T/T_c for EoS1 at $N_f = 3$ QGP. The potential is in the parallel condition ($\theta = 0$ degree). (b) Inner view of the minimum separation of panel (a). The black line with circles represents the results obtained from Nilima and Agotiya's EoS [82] and the red line with diamonds represents the results obtained from Solanki *et al.*'s EoS [38].

temperature is currently being studied by lattice QCD [89,90]. In Fig. 12 we have plotted the variation of pressure (P/T^4) with temperature (T/T_c) using EoS1 for $N_f = 3$ QGP along with Nilima and Agotiya's EoS [82] and Solanki *et al.*'s EoS [38]. Now, the energy density ϵ_s , the speed of sound (C_s^2), and so forth can be derived since we have obtained the pressure. In Fig. 13, we have plotted the energy density (ϵ_s/T^4) with the temperature (T/T_c) using EoS1 for $N_f = 3$ QGP along with Nilima and Agotiya's EoS [82] and Solanki *et al.*'s EoS [38]. In Fig. 14, we have plotted the speed of sound (C_s^2) with

temperature (T/T_c) using EoS1 for $N_f = 3$ QGP along with Nilima and Agotiya's EoS [82] and Solanki *et al.*'s EoS [38]. Our results of these thermodynamical properties of quark matter are approximately matched with the results of Nilima and Agotiya's EoS [82] and Solanki *et al.*'s EoS [38] with the anisotropy parameter. The effect of anisotropy was also observed in these thermodynamical properties of quark matter as shown in Figs. 12–14. If we increase the value of anisotropy ($\xi = 0$ to 0.3), then the variation of P/T^4 , ϵ_s/T^4 , and C_s^2 also increases slightly respectively [the panels (b) of Figs. 12–14

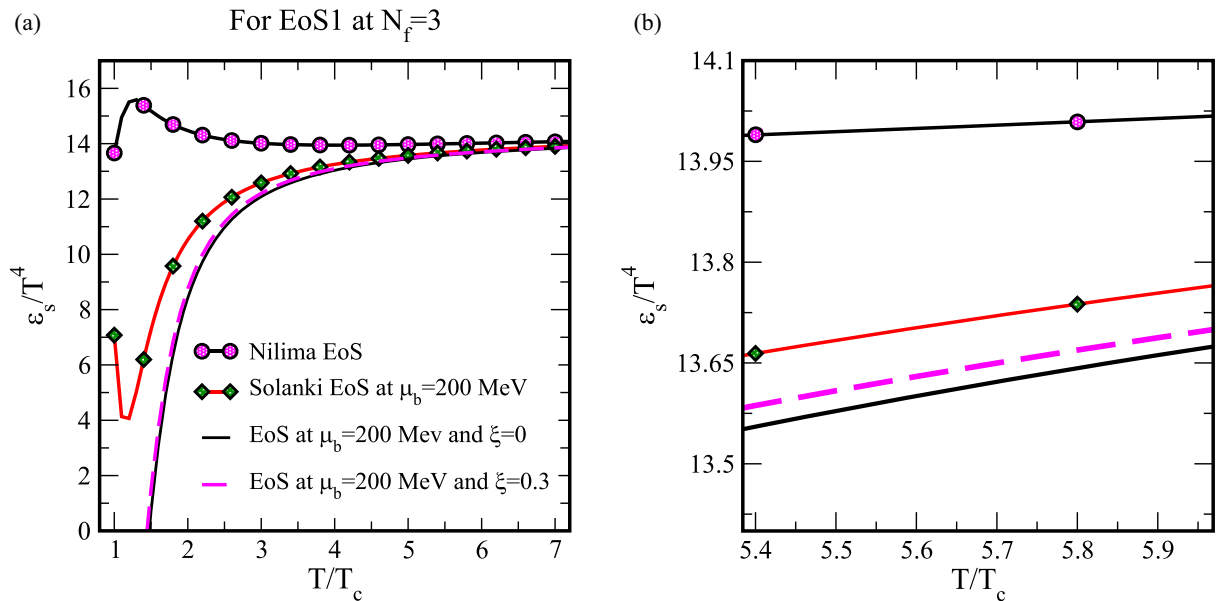


FIG. 13. (a) Variation of ϵ_s/T^4 with T/T_c for EoS1 at $N_f = 3$ QGP. The potential is in the parallel condition ($\theta = 0$ degree). (b) Inner view of the minimum separation of panel (a). The black line with circles represents the results obtained from Nilima and Agotiya's EoS [82] and the red line with diamonds represents the results obtained from Solanki *et al.*'s EoS [38].

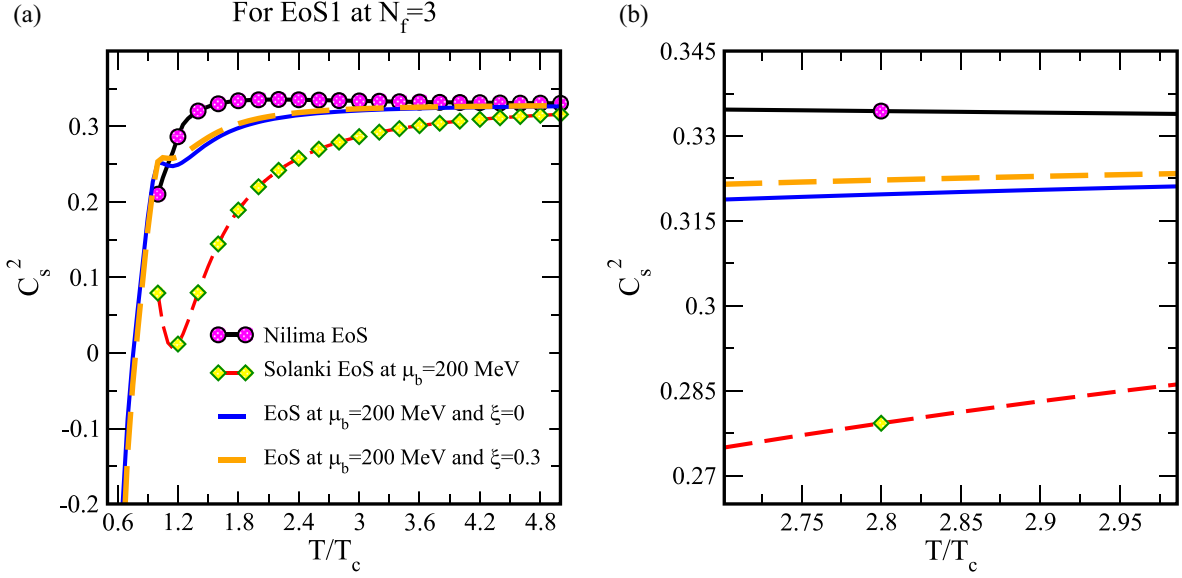


FIG. 14. (a) Variation of C_s^2 with T/T_c for EoS1 at $N_f = 3$ QGP. The potential is in the parallel condition ($\theta = 0$ degree). (b) Inner view of the minimum separation of panel (a). The black line with a circle represents the results obtained from Nilima and Agotiya's EoS [82] and the red line with diamonds represents the results obtained from Solanki *et al.*'s EoS [38].

show the minimum separation of the panels (a)]. Figure 15 shows the variation of P/T^4 with temperature (T/T_c) [panel (a)], ϵ_s/T^4 with temperature (T/T_c) [panel (b)] using EoS1 at $N_f = 3$, and C_s^2 with temperature (T/T_c) [panel (c)] using EoS1 at $N_f = 0$, and Fig. 15 also shows the lattice QCD results [82,83]. Because the lattice QCD (LQCD) results are available for only pure gauge, comparison [in Fig. 15] has been made for the abovementioned value of flavor N_f only. Our flavored results match approximately well with the LQCD results at $\xi = 0$ and $\mu_b = 0$. The main features are the sharp rise of the curves of P/T^4 , ϵ_s/T^4 , and C_s^2 around the value of critical temperature and then a linear curve to the ideal value. We have calculated these thermodynamical properties [i.e., P/T^4 , ϵ_s/T^4 , and C_s^2] to determine the hydrodynamical expansion of quark gluon plasma, and in the future we will extend our work to calculate the suppression of quarkonia in

nuclear collisions, taking into account the effect of anisotropy and the baryonic chemical potential.

IV. SUMMARY AND CONCLUSIONS

The present work is devoted to the study of the effect of the baryonic chemical potential (μ_b) on quarkonium properties in an anisotropic medium, by considering complex potentials having both a perturbative nature and a nonperturbative nature, using the quasiparticle Debye mass. It is known that anisotropy arises in primary stages as the system expands after the ultrarelativistic heavy ion-collision (URHIC) process. Under the condition $\xi = 0$, the string term (σ) of the Cornell potential makes the potential more attractive. This leads to the fact that respective quarkonium states become more bound in comparison to the case when the Coulombic term of the

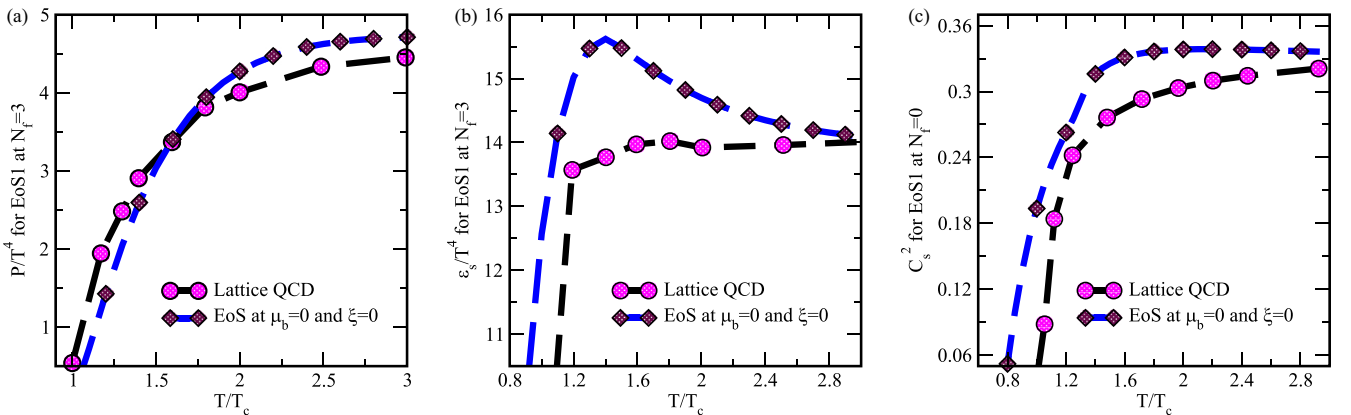


FIG. 15. Variation of P/T^4 with T/T_c (a), ϵ_s/T^4 with T/T_c (b) for EoS1 at $N_f = 3$, and C_s^2 with T/T_c (c) for EoS1 at $N_f = 0$ QGP. The potential is in the parallel condition ($\theta = 0$ degree). The black line with circles represents the lattice QCD results (for pure gauge) obtained from Ref. [82] and the blue line with diamonds represents our EoS at $\xi = 0$ and $\mu_b = 0$.

potential is modified alone. In this work, we have considered the values of anisotropy for three cases, viz., prolate ($\xi = -0.3$), isotropic ($\xi = 0$), and oblate ($\xi = 0.3$), with a fixed value of the critical temperature of $T_c = 197$ MeV.

We have reconsidered the medium-modified form of the heavy-quark potential at finite values of μ_b and ξ . This has been done by considering the real and imaginary parts of the potential with a static gluon propagator, which in turn gives the real and imaginary parts of the dielectric permittivity with the anisotropic parameter. We considered μ_b and the temperature-dependent quasiparticle Debye mass in the study of the dissociation pattern of quarkonia. The real part of the potential has been used for solving the Schrödinger equation to obtain the binding energy of quarkonia, and the imaginary part gives rise to the thermal width of heavy quarkonia. It was observed that the binding energy decreases and the thermal width increases with increasing the values of μ_b . However, the binding energy tends to get higher with increasing the value of ξ . In conclusion, the dissociation temperature of heavy quarkonia decreases with the baryonic chemical potential and increases with anisotropy as shown in Tables I–VI. The values of mass spectra were also calculated and it was noticed that, if we increase the values of μ_b , then the values of the mass spectra decrease, but if we increase the value of ξ , then the values of the mass spectra also increase. We also extend this work to calculate the thermodynamical properties of QGP with ξ and μ_b . These EoSs are important to study the suppression phenomena in the presence of ξ and μ_b . We have also extended this work, after calculating the thermodynamical properties of QGP (i.e., pressure, energy density, and speed of sound) using ξ and μ_b , mainly for the calculation of nucleus-nucleus suppression with the effect of anisotropy and the baryonic chemical potential. It was observed that, if we increase the values of ξ from 0 to 0.3, the variation of the pressure, the energy density, and the speed of sound with T/T_c increases a little bit.

In the future, we will extend this work to calculate the survival property of different quarkonium states in the presence of ξ and μ_b at different states of energy density ($\sqrt{s_{NN}}$). This survival probability will be calculated with respect to anisotropy, the baryonic chemical potential, the transverse momentum, centrality, and rapidity, which is the key point to quantify various properties of the medium produced during heavy-ion collisions at the LHC and the RHIC. The results of this work might be helpful for expanding the studies of highly dense objects like neutron stars. Because the Compressed Baryonic Matter (CBM) experiment at the Facility for Antiproton and Ion Research (FAIR) is exploring QGP at higher baryon densities, this type of theoretical study may contribute to our understanding of the physics of highly dense bodies with high baryon densities.

APPENDIX: CALCULATIONS FOR THE REAL AND IMAGINARY PARTS OF THE TEMPORAL COMPONENT OF THE PROPAGATOR

An advantageous representation of propagators in a real-time formalism is the Keldysh representation where the four-components of the matrix form are in linear combination; among these four-components of the matrix, three-

components are independent, giving the relation for advanced (A), retarded (R) and symmetric (F) propagators, respectively,

$$D_R^0 = D_{11}^0 - D_{12}^0, \quad D_A^0 = D_{11}^0 - D_{21}^0, \quad D_F^0 = D_{11}^0 - D_{22}^0. \quad (\text{A1})$$

In the distribution function, only F components are involved and they are particularly useful for the HTL diagrams. Similar relations for the self-energies are

$$\Pi_R = \Pi_{11} + \Pi_{12}, \quad \Pi_A = \Pi_{11} + \Pi_{21}, \quad \Pi_F = \Pi_{11} + \Pi_{22}. \quad (\text{A2})$$

Resuming the Dyson-Schwinger equation, the R , A , and F propagators can be written as

$$D_{R,A} = D_{R,A}^0 + D_{R,A}^0 \Pi_{R,A} D_{R,A} \quad (\text{A3})$$

and

$$D_F = D_F^0 + D_R^0 \Pi_R D_F + D_F^0 \Pi_A D_A + D_R^0 \Pi_F D_A. \quad (\text{A4})$$

Now place the F propagator $D_F^0(P)$ in terms of the R and A propagators, then the resummed F propagators are

$$\begin{aligned} D_F(P) &= (1 + 2f_B) \text{sgn}(p_0) [D_R(P) - D_A(P)] \\ &\quad + D_R(P) \{ \Pi_F(P) - (1 + 2f_B) \text{sgn}(p_0) \\ &\quad \times [\Pi_R(P) - \Pi_A(P)] \} D_A(P). \end{aligned} \quad (\text{A5})$$

For the calculation of the static potential in the $\xi = 0$ medium, only the temporal (L) component of the propagator is required, so the R and A propagators in the form of the simplest Coulomb gauge are

$$D_{R,A}^L(\text{iso}) = D_{R,A}^{L(0)} + D_{R,A}^{L(0)} \Pi_{R,A}^L D_{R,A}^L(\text{iso}). \quad (\text{A6})$$

Now, we first enhance the self-energy and propagators around the $\xi = 0$ limit and withhold only the linear term:

$$D = D_{\text{iso}} + \xi D_{\text{aniso}}, \quad \Pi = \Pi_{\text{iso}} + \xi \Pi_{\text{aniso}} \quad (\text{A7})$$

The L component of the R and A propagators in the presence of small ξ becomes

$$\begin{aligned} D_{R,A}^L(\text{aniso}) &= D_{R,A}^{L(0)} \Pi_{R,A}^L D_{R,A}^L(\text{iso}) \\ &\quad + D_{R,A}^{L(0)} \Pi_{R,A}^L D_{R,A}^L(\text{aniso}), \end{aligned} \quad (\text{A8})$$

whereas the notations for the difference of self-energies and the propagators can be obtained [11,46]. For the solution of the propagators, now we calculate the gluon self-energy for the gluon and quark loops [11] with external and internal momenta, respectively, with $Q = K - P$:

$$\Pi^{\mu\nu}(P) = -\frac{i}{2} N_f g^2 \int \frac{d^4 K}{(2\pi)^4} \text{tr}[\gamma^\mu S(Q) \gamma^\nu S(K)], \quad (\text{A9})$$

and the R self-energy is

$$\begin{aligned} \Pi_R^{\mu\nu}(P) &= -\frac{i}{2} N_f g^2 \int \frac{d^4 K}{(2\pi)^4} \{ \text{tr}[\gamma^\mu S_{11}(Q) \gamma^\nu S_{11}(K)] \\ &\quad - \text{tr}[\gamma^\mu S_{21}(Q) \gamma^\nu S_{12}(K)] \}. \end{aligned} \quad (\text{A10})$$

In the limit of massless quarks, the longitudinal part of the self-energy is

$$\begin{aligned} & \frac{\Pi_R^L(P)}{-iN_f g^2 \int \frac{d^4 K}{(2\pi)^4} (q_0 k_0 + \mathbf{q} \cdot \mathbf{k})} \\ &= [\tilde{\Delta}_F(Q)\tilde{\Delta}_R(K) + \tilde{\Delta}_A(Q)\tilde{\Delta}_F(K)] \\ &+ [\tilde{\Delta}_A(Q)\tilde{\Delta}_A(K) + \tilde{\Delta}_R(Q)\tilde{\Delta}_R(K)]. \end{aligned} \quad (\text{A11})$$

In the weak-coupling limit, the external momentum is much lower than the internal momentum, so the R self-energy in the HTL approximation simplifies to [11]

$$\Pi_R^L(P) = \frac{4\pi N_f g^2}{(2\pi)^4} \int k dk \int d\Omega f_F(\mathbf{k}) \frac{1 - (\hat{\mathbf{k}} \cdot \hat{\mathbf{p}})^2}{(\hat{\mathbf{k}} \cdot \hat{\mathbf{p}} + \frac{p_0 + i\epsilon}{p})^2}. \quad (\text{A12})$$

After elaborating the distribution function, in a weakly anisotropic (ξ is not equal to 0) medium, the R quark self-energy becomes

$$\Pi_R^L(P) = \frac{g^2}{(2\pi)^2} N_f \sum_{i=0}^1 \int_0^\infty k \Phi_{(i)}(k) dk \int_{-1}^1 \Psi_{(i)}(s) ds, \quad (\text{A13})$$

with

$$\Phi_{(0)}(k) = n_F(k), \quad (\text{A14})$$

$$\Phi_{(1)}(k) = -\xi n_F^2(k) \frac{ke^{k/T}}{2T}, \quad (\text{A15})$$

$$\Psi_{(0)}(s) = \frac{1 - s^2}{(s + \frac{p_0 + i\epsilon}{p})^2}, \quad (\text{A16})$$

and

$$\Psi_{(1)}(s) = \cos^2 \theta_p \frac{s^2(1 - s^2)}{(s + \frac{p_0 + i\epsilon}{p})^2} + \frac{\sin^2 \theta_p}{2} \frac{(1 - s^2)^2}{(s + \frac{p_0 + i\epsilon}{p})^2}. \quad (\text{A17})$$

Here, the angle θ_p is defined as the angle between \mathbf{n} and \mathbf{p} and $s = \hat{\mathbf{k}} \cdot \hat{\mathbf{p}}$. After spoiling into anisotropic pieces, the anisotropic and $\xi = 0$ (isotropic) terms become

$$\begin{aligned} \Pi_{R(\text{aniso})}^L(P) &= N_f \frac{g^2 T^2}{6} \left(\frac{1}{6} + \frac{\cos 2\theta_p}{2} \right), \\ &+ \Pi_{R(\text{iso})}^L(P) \left(\cos 2\theta_p - \frac{p_0^2}{2p^2} (1 + 3 \cos 2\theta_p) \right), \end{aligned} \quad (\text{A18})$$

and

$$\Pi_{R(\text{iso})}^L(P) = N_f \frac{g^2 T^2}{6} \left(\frac{p_0}{2p} \ln \frac{p_0 + p \pm i\epsilon}{p_0 - p \pm i\epsilon} - 1 \right). \quad (\text{A19})$$

Thus, the gluon self-energy found both imaginary and real parts, which are accountable for Landau damping and Debye screening, respectively, which are usually obtained from the R and advanced self-energy and later are obtained from the F self-energy alone.

-
- [1] J. Adams *et al.* (STAR Collaboration), *Nucl. Phys. A* **757**, 102 (2005); K. Adcox *et al.* (PHENIX Collaboration), *ibid.* **757**, 184 (2005); B. B. Back *et al.* (PHOBOS Collaboration), *ibid.* **757**, 28 (2005); I. Arsene *et al.* (BRAHMS Collaboration), *ibid.* **757**, 1 (2005).
- [2] K. Aamodt *et al.* (Alice Collaboration), *Phys. Rev. Lett.* **105**, 252302 (2010); **105**, 252301 (2010); **106**, 032301 (2011).
- [3] U. W. Heinz, Cern yellow report CERN-2004-001, pp. 127–178, [arXiv:hep-ph/0407360](https://arxiv.org/abs/hep-ph/0407360).
- [4] U. Kakade and B. K. Patra, *Phys. Rev. C* **92**, 024901 (2015).
- [5] J. E. Augustin *et al.* (SLAC-SP-017 Collaboration), *Phys. Rev. Lett.* **33**, 1406 (1974).
- [6] T. Matsui and H. Satz, *Phys. Lett. B* **178**, 416 (1986).
- [7] B. K. Patra, V. Agotiya, and Vinod Chandra, *Eur. Phys. J. C* **67**, 465 (2010).
- [8] S. Datta, F. Karsch, P. Petreczky, and I. Wetzorke, *Phys. Rev. D* **69**, 094507 (2004).
- [9] N. Brambilla, J. Ghiglieri, A. Vairo, and P. Petreczky, *Phys. Rev. D* **78**, 014017 (2008).
- [10] Y. Burnier, M. Laine, and M. Vepsäläinen, *Phys. Lett. B* **678**, 86 (2009).
- [11] A. Dumitru, Y. Guo, and M. Strickland, *Phys. Rev. D* **79**, 114003 (2009).
- [12] M. Laine, O. Philipsen, P. Romatschke, and M. Tassler, *J. High Energy Phys.* **03** (2007) 054.
- [13] E. Eichten, S. Godfrey, H. Mahlke, and J. L. Rosner, *Rev. Mod. Phys.* **80**, 1161 (2008).
- [14] M. B. Voloshin, *Prog. Part. Nucl. Phys.* **61**, 455 (2008).
- [15] C. Patrignani, T. K. Pedlar, and J. L. Rosner, *Annu. Rev. Nucl. Part. Sci.* **63**, 21 (2013).
- [16] N. Brambilla *et al.*, *Eur. Phys. J. C* **71**, 1534 (2011).
- [17] E. L. Berger, J. W. Qiu, and Y. L. Wang, *Phys. Rev. D* **71**, 034007 (2005).
- [18] E. L. Berger and D. L. Jones, *Phys. Rev. D* **23**, 1521 (1981).
- [19] R. Rapp, D. Blaschke, and P. Crochet, *Prog. Part. Nucl. Phys.* **65**, 209 (2010).
- [20] C. Silvestre (PHENIX Collaboration), *J. Phys. G: Nucl. Part. Phys.* **35**, 104136 (2008).
- [21] F. Scardina, M. Colonna, S. Plumari, and V. Greco, *Phys. Lett. B* **724**, 296 (2013).
- [22] W. E. Caswell and G. P. Lepage, *Phys. Lett. B* **167**, 437 (1986).
- [23] A. Pineda, *Prog. Part. Nucl. Phys.* **67**, 735 (2012).
- [24] H. S. Shao, H. Han, Y. Q. Ma, C. Meng, Y. J. Zhang, and K. T. Chao, *J. High Energy Phys.* **05** (2015) 103.
- [25] A. Adare *et al.* (PHENIX Collaboration), *Phys. Rev. C* **84**, 054912 (2011).
- [26] J. A. López López (ATLAS Collaboration), *Nucl. Phys. A* **967**, 584 (2017).
- [27] Q. Hu (ATLAS Collaboration), *Nucl. Phys. A* **956**, 685 (2016).
- [28] D. Thakur, S. De, R. Sahoo, and S. Dansana, *Phys. Rev. D* **97**, 094002 (2018).

- [29] B. Duclou, T. Lappi, and H. Mntysaari, *Nucl. Part. Phys. Proc.* **289-290**, 309 (2017).
- [30] N. Brambilla, A. Pineda, J. Soto, and A. Vairo, *Rev. Mod. Phys.* **77**, 1423 (2005); N. Brambilla, M. A. Escobedo, J. Ghiglieri, and A. Vairo, *J. High Energy Phys.* **05** (2013) 130.
- [31] J. Geiss, C. Greiner, E. L. Bratkovskaya, W. Cassing, and U. Mosel, *Phys. Lett. B* **447**, 31 (1999).
- [32] V. K. Agotiya, V. Chandra, M. Y. Jamal, and I. Nilima, *Phys. Rev. D* **94**, 094006 (2016).
- [33] M. Martinez and M. Strickland, *Phys. Rev. Lett.* **100**, 102301 (2008); *Phys. Rev. C* **78**, 034917 (2008).
- [34] R. Baier and Y. Mehtar-Tani, *Phys. Rev. C* **78**, 064906 (2008).
- [35] V. Chandra and V. Ravishankar, *Phys. Rev. D* **84**, 074013 (2011).
- [36] M. E. Carrington, K. Deja, and S. Mrowczynski, *Phys. Rev. C* **90**, 034913 (2014).
- [37] S. Solanki, M. Lal, and V. K. Agotiya, *Adv. High Energy Phys.* **2022**, 1456538 (2022).
- [38] S. Solanki, M. Lal, R. Sharma, and V. K. Agotiya, *Int. J. Mod. Phys. A* **37**, 2250196 (2022).
- [39] M. Yousuf Jamal, S. Mitra, and V. Chandra, *Phys. Rev. D* **95**, 094022 (2017).
- [40] Y. Burnier, M. Laine, and M. Vepsalainen, *J. High Energy Phys.* **01** (2008) 043.
- [41] A. Beraudo, J. P. Blaizot, and C. Ratti, *Nucl. Phys. A* **806**, 312 (2008).
- [42] M. Laine, O. Philipsen, and M. Tassler, *J. High Energy Phys.* **09** (2007) 066; T. Hatsuda, *Nucl. Phys. A* **904-905**, 210c (2013).
- [43] M. Margotta, K. McCarty, C. McGahan, M. Strickland, and D. Yager-Elorriaga, *Phys. Rev. D* **83**, 105019 (2011).
- [44] M. Strickland and D. Bazow, *Nucl. Phys. A* **25**, 879 (2012).
- [45] L. Thakur, U. Kakade, and B. K. Patra, *Phys. Rev. D* **89**, 094020 (2014).
- [46] A. Mocsy and P. Petreczky, *Phys. Rev. Lett.* **99**, 211602 (2007).
- [47] M. A. Escobedo and J. Soto, *Phys. Rev. A* **78**, 032520 (2008).
- [48] A. K. Rebhan *et al.*, *Phys. Rev. D* **48**, R3967 (1993).
- [49] E. Braaten and A. Nieto, *Phys. Rev. Lett.* **73**, 2402 (1994).
- [50] P. Arnold and C. Zhai, *Phys. Rev. D* **51**, 1906 (1995).
- [51] K. Kajantie, M. Laine, J. Peisa, A. Rajantie, K. Rummukainen, and M. E. Shaposhnikov, *Phys. Rev. Lett.* **79**, 3130 (1997).
- [52] S. Nadkarni, *Phys. Rev. D* **33**, 3738 (1986); **34**, 3904 (1986).
- [53] Y. Burnier and A. Rothkopf, *Phys. Lett. B* **753**, 232 (2016).
- [54] V. Goloviznin and H. Satz, *Z. Phys. C* **57**, 671 (1993).
- [55] A. Peshier, B. Kampfer, O. P. Pavlenko, and G. Soff, *Phys. Rev. D* **54**, 2399 (1996).
- [56] M. D'Elia, A. Di Giacomo, and E. Meggiolaro, *Phys. Lett. B* **408**, 315 (1997); *Phys. Rev. D* **67**, 114504 (2003).
- [57] A. Dumitru and R. D. Pisarski, *Phys. Lett. B* **525**, 95 (2002).
- [58] V. Chandra, R. Kumar, and V. Ravishankar, *Phys. Rev. C* **76**, 054909 (2007).
- [59] V. Chandra, A. Ranjan, and V. Ravishankar, *Eur. Phys. J. A* **40**, 109 (2009).
- [60] P. K. Srivastava, S. K. Tiwari, and C. P. Singh, *Phys. Rev. D* **82**, 014023 (2010).
- [61] W. Lucha *et al.*, *Phys. Rep.* **200**, 127 (1991).
- [62] V. Agotiya, V. Chandra, and B. K. Patra, *Phys. Rev. C* **80**, 025210 (2009).
- [63] R. A. Schneider, *Phys. Rev. D* **66**, 036003 (2002).
- [64] H. A. Weldon, *Phys. Rev. D* **26**, 1394 (1982).
- [65] A. Ranjan and V. Ravishankar, arXiv:0707.3697.
- [66] H. Satz, *J. Phys. G: Nucl. Part. Phys.* **32**, R25 (2006).
- [67] V. V. Dixit, *Mod. Phys. Lett. A* **5**, 227 (1990).
- [68] P. Romatschke and M. Strickland, *Phys. Rev. D* **68**, 036004 (2003).
- [69] A. V. Luchinsky, *Mod. Phys. Lett. A* **33**, 1850001 (2018).
- [70] A. K. Likhoded, A. V. Luchinsky, and S. V. Poslavsky, *JETP Lett.* **105**, 739 (2017).
- [71] S. Aronson, E. Borrás, B. Odegard, R. Sharma, and I. Vitev, *Phys. Lett. B* **778**, 384 (2018).
- [72] M. H. Thoma, arXiv:hep-ph/0010164.
- [73] E. Braaten and R. D. Pisarski, *Nucl. Phys. B* **337**, 569 (1990).
- [74] J. P. Blaizot and E. Iancu, *Nucl. Phys. B* **417**, 608 (1994).
- [75] P. F. Kelly, Q. Liu, C. Lucchesi, and C. Manuel, *Phys. Rev. D* **50**, 4209 (1994).
- [76] M. Strickland and D. Bazow, *Nucl. Phys. A* **879**, 25 (2012).
- [77] D. Kharzeev, L. D. McLerran, and H. Satz, *Phys. Lett. B* **356**, 349 (1995).
- [78] M. Lal, S. Solanki, R. Sharma, and V. K. Agotiya, *Adv. High Energy Phys.* **2023**, 6922729 (2023).
- [79] M. Tanabashi, K. Hagiwara, K. Hikasa *et al.* (Particle Data Group), *Phys. Rev. D* **98**, 030001 (2018).
- [80] D. Pal, B. K. Patra, and D. K. Srivastava, *Eur. Phys. J. C* **17**, 179 (2000).
- [81] B. K. Patra and D. K. Srivastava, *Phys. Lett. B* **505**, 113 (2001).
- [82] I. Nilima and V. K. Agotiya, *Adv. High Energy Phys.* **2019**, 9574136 (2019).
- [83] V. M. Bannur, *J. Phys. G: Nucl. Part. Phys.* **32**, 993 (2006); G. Boyd, J. Engels, F. Karsch, E. Laermann, C. Legeland, M. Lutgemeier, and B. Petersson, *Phys. Rev. Lett.* **75**, 4169 (1995); *Nucl. Phys. B* **469**, 419 (1996); A. Bavavov *et al.*, *Phys. Rev. D* **80**, 014504 (2009).
- [84] S. Ichimaru, *Statistical Plasma Physics*, Vol. II: *Condensed Plasma* (Addison-Wesley, New York, 1994).
- [85] S. Ichimaru, *Rev. Mod. Phys.* **54**, 1017 (1982).
- [86] M. Laine and Y. Schroder, *J. High Energy Phys.* **03** (2005) 067.
- [87] S. Huang and M. Lissia, *Nucl. Phys. B* **438**, 54 (1995).
- [88] E. Braaten and A. Nieto, *Phys. Rev. D* **53**, 3421 (1996).
- [89] S. Plumari, W. M. Alberico, V. Greco, and C. Ratti, *Phys. Rev. D* **84**, 094004 (2011).
- [90] H. Berrehrah, E. Bratkovskaya, T. Steinert, and W. Cassing, *Int. J. Mod. Phys. E* **25**, 1642003 (2016).